nature communications

Article

https://doi.org/10.1038/s41467-024-52510-3

A point mutation in *VIG1* boosts development and chilling tolerance in rice

Received: 5 March 2024

Accepted: 11 September 2024

Published online: 18 September 2024

Check for updates

Dunpin Xiong[1,2], Juan Wang[3], Ruci Wang[1], Yueming Wang[1], Yi Li[1,2], Ge Sun[1,2] & Shanguo Yao[1]

The rice paddy-direct seeding system has been widely adopted due to its low cost and convenience, whereas its application is mainly constrained by low seedling vigor, cold sensitivity, eventually resulting in reduced grain yield. Here, we show *vig1a* and *vig1b*, two allelic mutants of *OsbZIP01*, that both demonstrate greatly enhanced seedling vigor and chilling tolerance but differ in final grain production. The *vig1a* phenotype can be obtained via simultaneous mutation of the genes *OsbZIP01* and *OsbZIP18*, or by selectively manipulating the basic region of OsbZIP01. Destroying the leucine zipper region of OsbZIP01 in *vig1a* turns *vig1a* to be *vig1b*. Further analysis reveals that OsbZIP01 and OsbZIP18 function cooperatively in diverse crucial biological programs that determine seedling establishment, chilling tolerance, and grain yield through their interactions. These findings provide a strategy toward simultaneously improving seedling vigor, chilling tolerance, and grain yield for rice production.

Rice (*Oryza sativa* L.) is the staple food for over half of the world's population[1]. Considering factors such as accelerated aging of the global population, severe labor shortages, and gradually rising production costs, global food production faces serious challenges[2,3]. Recently, direct-seeding, especially the paddy direct-seeding system has been widely adopted for growing rice because of the decreased agricultural production costs, reduced labor input and shorter rice lifecycle compared with traditional transplanting[4], which rely much on the seedling vigor, chilling tolerance and high productivity of rice cultivars. Unfortunately, the origination and domestication in tropical and subtropical regions have caused modern rice varieties to have greatly reduced seedling vigor and exhibit extreme sensitivity to cold at various developmental stages[5–7]. Worse still, direct seeding is associated with markedly reduced grain production and this is due to sloppy field management[5,8]. Thus, expanding the application of this system calls for the need to identify regulators that improve all three parameters, namely, seedling vigor, chilling tolerance, and grain yield.

Seedling vigor (SV), which is mainly characterized by the rapid early growth of both the shoots and roots, is a complex agronomic trait that is controlled by numerous quantitative genetic loci (QTLs)[9–11]. Through map-based cloning and genome-wide association study, many QTLs associated with shoot and/or root length have been identified[12–15]. One of them, which is soil-surface rooting 1 (SOR1), modulates the stability of Aux/IAA protein, thereby inhibiting the growth of rice roots in length[14]. On the other hand, OsSWEET3a exerts dual functions as a gibberellin and glucose transporter, resulting in proper young shoot development[15]. However, little is known about how seedlings coordinate growth with stress response to adapt to their surrounding environment. Chilling tolerance (CT) is another fundamental factor that affects paddy direct-seeding. Additionally, rice is sensitive to chilling stress at various developmental stages, and the genes associated with this trait have been extensively elucidated[16–19]. It has been reported that several genes simultaneously regulate SV and CT, both of which are vital for the establishment of rice plants and survival under chilling stress conditions[20–23]. For example, OsICE1 activates the expression of *OsTPP1* through being phosphorylated by OsMAPK3, eventually promoting shoot growth and CT[20]. *OsMADS57* is another target that positively modulates CT and growth in seedlings[21]. OsCYP20-2, which is a variant of cyclophilin, interacts with SLENDER RICE1 (SLR1) and

[1]State Key Laboratory of Plant Genomics, Institute of Genetics and Developmental Biology, The Innovative Academy of Seed Design, Chinese Academy of Sciences, Beijing 100101, China. [2]College of Advanced Agricultural Sciences, University of Chinese Academy of Sciences, Beijing 100039, China. [3]Maize Research Institute, Shandong Academy of Agricultural Sciences, Jinan 250100, China. e-mail: sgyao@genetics.ac.cn

OsFSD, resulting in reduced growth and CT of seedlings[22]. OsGRF6 also positively regulates seedling growth but negatively controls CT by interacting with SLR1 to regulate the expression of *OsGA2ox1* at different ambient temperatures[23]. Although some research has been done on the simultaneous control of SV and CT, little attention has been paid to the effects of various regulators on grain yield.

As a crucial crop plant, rice production is mainly determined by grain number per panicle (GNP), tiller number per plant, and grain weight. Therefore, more research is focusing on improving rice production by targeting these parameters[24]. GNP shaped by the primary and secondary branches makes the most significant contributions to grain yield[25]. Over the past decades, several major QTLs associated with the rice GNP have been identified and show great potential for breeding high-yield varieties[26–28]. For example, *Gn1a*/*OsCKX2* is identified to modulate GNP, and it functions as an enzyme that degrades cytokinin, a crucial phytohormone[26]. *DEP1* is another target that is involved in regulating meristematic activity and final GNP[27]. Additionally, *IDEAL PLANT ARCHITECTURE 1* (*IPA1*) targeted by microRNA (miRNA) OsmiR156 defines the architecture of rice plants with enhanced GNP[28]. Although many regulators that control SV, CT, and GNP as individual traits have been identified, few have been reported to balance all of them. So far, *IPA1* has been reported to be the vital target that integrate SV, CT, and GNP[28–30], loss function of *IPA1* attenuates rice CT and GNP but promotes SV[28–30]. Therefore, more research is required to identify regulators and elucidate the mechanism underlying the tradeoff between SV, CT, and GNP, which will be greatly beneficial in rice breeding.

In this study, we report the identification of *vig1a*, a mutant that exhibits significantly enhanced SV, CT, and GNP. The causal mutation is localized to be *OsbZIP01*. VIG1 (OsbZIP01), together with OsbZIP18, which is another bZIP TF, synergistically suppresses the expression of genes involved in cell expansion and proliferation, as well as the C-REPEAT BINDING FACTOR/DEHYDRATION-RESPONSIVE ELEMENT-BINDING PROTEIN (CBF/DREB) pathway and GNP control, thereby promoting simultaneously SV, CT, and GNP. Our results introduce an approach to synergistic optimum mechanisms for high-yield crops by improving rice SV, CT, and GNP.

Results

Characterization of two allelic mutants and isolation of *VIG1*

By screening a NaN_3-mutagenized M_2 library under the background of KY131 (*japonica*), we identified a mutant with elongated shoots, coleoptiles, and seminal roots at different time points after germination (Fig. 1a–c; Supplementary Fig. 1a), and designated *vig1a* (for *vigorous 1a*). Cytological analysis showed that the coleoptile inner cell length of *vig1a* is 1.6 times that of the wide-type (WT), but the cell width remains unchanged (Supplementary Fig. 1b, c). However, the coleoptile length of *vig1a* is 1.8 times that of the WT (Supplementary Fig. 1a). This indicates that the elongated shoots of *vig1a* are due to simultaneously elevated cell elongation and proliferation. After four days of chilling stress treatment, *vig1a* presented a survival rate of 74.2%, sharply contrasting the 0.83% for the WT (Fig. 1d, g). The heading date of *vig1a* was 85 days, which is later compared to the 71 days for the WT (Fig. 1h; Supplementary Fig. 1d). In addition, increased plant height and GNP were associated with *vig1a* (Fig. 1e, f, i, j). These findings suggest that *vig1a* confers enhanced SV, CT, and GNP.

Given that great differences in SV, CT, and GNP were also observed between KD8 (*japonica*) and *vig1a* (Supplementary Fig. 2a–d, f–i), *VIG1* was located by conducting a cross between these two materials. The candidate gene was initially mapped to the short arm of chromosome 1 between markers M1 and M2 (Fig. 1k) using 20 bulked WT and mutant plants from the F_2 population (Supplementary Fig. 2e) between *vig1a* and KD8. Further analysis of 1920 plants with the mutant phenotype (longer primary roots) narrowed down the causal gene to a 90-kb region between markers M5 and M6, which comprises 13 annotated genes (Fig. 1k). After sequencing the fine-mapped region, guanine (G) to adenine (A) point mutation was identified in the second exon of the gene *OsbZIP01* (Fig. 1k; Supplementary Fig. 1e; http://rice.plantbiology.msu.edu/) in *vig1a*, resulting in the substitution of arginine 121 to histidine (R121H) in the basic region of its encoded protein (Fig. 1k; Supplementary Fig. 1f, g). To confirm the mapping result, a 3.52 kb genomic sequence of *OsbZIP01*, including the entire coding region, 2198-bp upstream of ATG and 542-bp downstream of TAG, was amplified from WT and introduced into *vig1a*. After transformation, the mutant phenotype of *vig1a*, including SV, CT, heading date, and GNP was fully rescued in the independent T_3 positive transgenic plants (Supplementary Fig. 3), indicating that *OsbZIP01* is responsible for *vig1a*.

Further research revealed another NaN_3-treated mutant *vig1b* (KY131 background). Comparisons with WT showed that *vig1b* had remarkably elongated shoots and seminal roots on different days after germination, in addition to significantly enhanced CT (Fig. 1l-n; Supplementary Fig. 4a, d). The heading date of *vig1b* was comparable to the WT, though the plant height and GNP were lower (Supplementary Fig. 1d, 4b, c, e–g). Given the high similarities of *vig1a* and *vig1b* in both SV and CT, a cross was conducted between them, and F_1 plants showed *vig1a* phenotype. This indicates that *vig1a* is allelic and dominant to *vig1b*. Therefore, we sequenced gene *OsbZIP01* in *vig1b* and discovered a 14 bp deletion in the second exon, which resulted in a frameshift mutation of OsbZIP01 (Supplementary Fig. 4h, j, k). This observation was further confirmed by PCR-based agarose gel electrophoresis (Supplementary Fig. 4i), suggesting that *vig1b* is another mutant of *OsbZIP01*. To verify the 14 bp deletion was responsible for *vig1b*, the aforementioned 3.52 kb genomic sequence of WT was introduced into *vig1b* and transformed. Consistently, all the independent T_3 complementary lines resembled the WT phenotype as far as SV, CT, and GNP traits are concerned (Supplementary Fig. 5), indicating that *OsbZIP01* is the causal gene underlying *vig1b*. To validate that *vig1a* is dominant to *vig1b*, the 3.52 kb genomic sequence was amplified from *vig1a* and introduced into *vig1b*. A total of 32 independent T_3 complementary lines were obtained and they presented the *vig1a* phenotype (Supplementary Fig. 6). These results indicated that *vig1a* is completely dominant to *vig1b*, making the former a good candidate for the simultaneous improvement of SV, CT, and GNP.

Different transgenic plants of *VIG1* fail to mimic the *vig1a* phenotype

To determine the function of *VIG1*, a target site was designed at the front end of the second exon (*VIG1*-NK) of *OsbZIP01* (Supplementary Fig. 7a), before knocking it out in KY131 using the CRISPR/Cas9 genome editing tool[31]. Two homozygous lines with a 1-bp insertion (*VIG1*-NK1) and a 2-bp deletion (*VIG1*-NK2) in the coding region were selected (Supplementary Fig. 7a), both of which resulted in a frameshift mutation of VIG1 (Supplementary Fig. 8), for phenotypic analysis. Surprisingly, the SV and CT of both *VIG1*-NK lines were comparable to KY131 (Supplementary Fig. 7b, c, e–g). Additionally, significantly reduced GNP was observed in both *VIG1*-NK lines (Supplementary Fig. 7d, h). To further verify the function of *OsbZIP01* in SV, CT, and GNP, another target site at the posterior end of the second exon (*VIG1*-CK1) was edited to knock it out in KY131 (Fig. 2a). Two homozygous lines with a 1-bp insertion (*VIG1*-CK1-1) and a 42-bp deletion (*VIG1*-CK1-2) in the coding region were identified. The former caused a frameshift mutation, while the latter resulted in a 13 amino acid (aa) deletion in the leucine zipper region of VIG1 (Supplementary Fig. 9). Both lines presented phenotypes with remarkably enhanced SV and CT but decreased GNP, similar to *vig1b* (Fig. 2a–h). The findings suggested functional divergence in different regions of *OsbZIP01*.

To decipher whether the phenotype of *VIG1*-CK is material-specific, the same target site was selected as shown in Fig. 2a, and *OsbZIP01* was knocked out in KD8 (Supplementary Fig. 10a).

https://doi.org/10.1038/s41467-024-52510-3

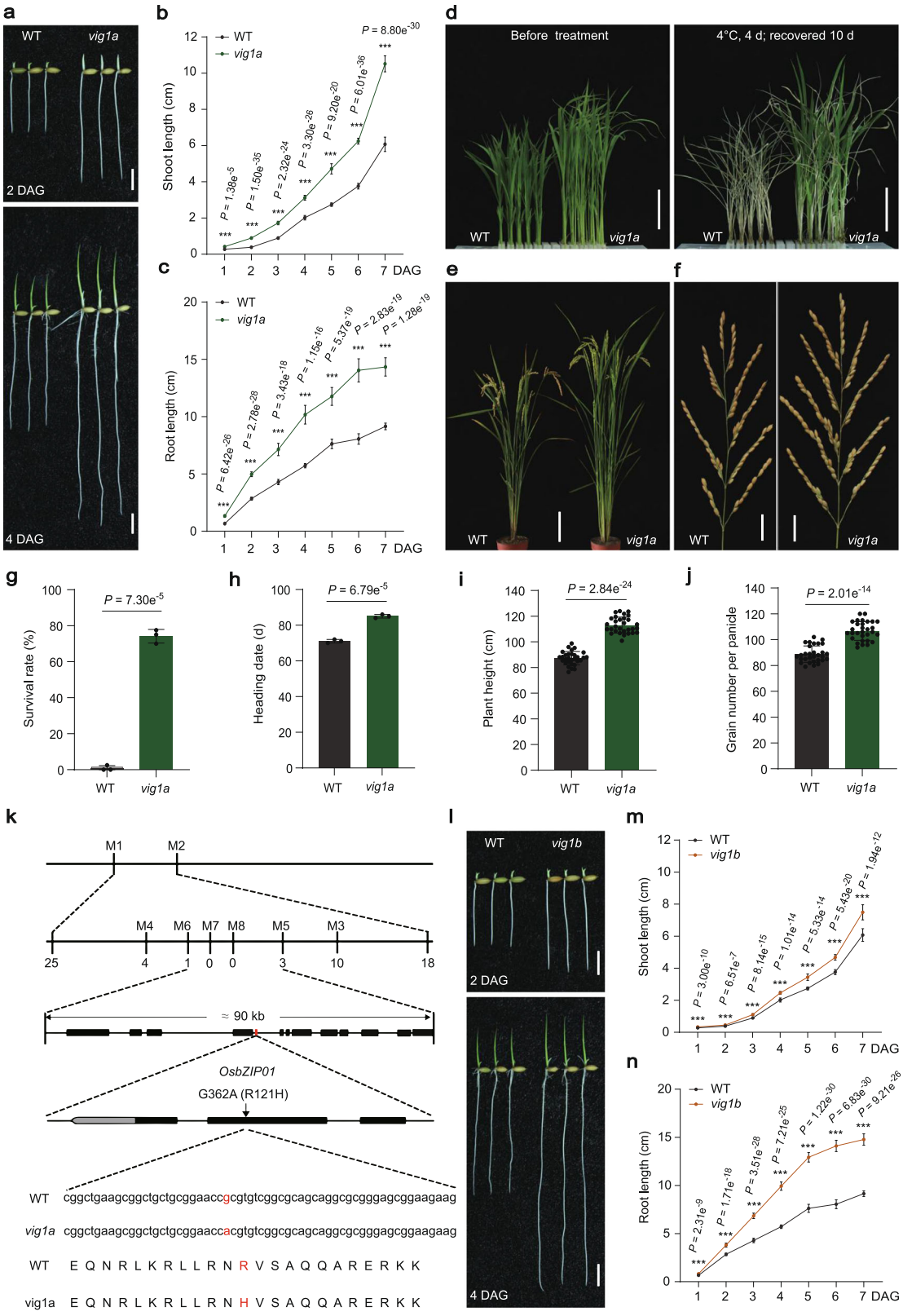

Two homozygous lines with a 1-bp insertion (*VIG1*-CK2-1) and a 2-bp deletion (*VIG1*-CK2-2) in the coding region caused frameshift mutations of VIG1 (Supplementary Fig. 11). Both lines showed significantly elevated SV and CT, as well as lower GNP (Supplementary Fig. 10a–h). These results were consistent with what has been observed in KY131, indicating that *VIG1*-CK is not material-specific and can fully mimic the *vig1b* phenotype. In addition, the overexpression of *VIG1* remarkably reduced the shoot length but increased seminal root length, compared to the wide-type KY131 (Supplementary Fig. 12a–c, e), whereas the CT of various lines was significantly reduced (Supplementary Fig. 12d, f). Overexpression of *VIG1* also delayed flowering by 13–15 days, in addition to increasing the plant height and GNP for different lines, in comparison with KY131 (Supplementary Fig. 12g–j). These results indicate that *VIG1* plays a complicated role in regulating SV, CT and

Fig. 1 | Characterization of mutants *vig1a* and *vig1b*, and isolation of *VIG1*. **a** Seedling morphology of WT and *vig1a*. Scale bars, 1 cm. **b**, **c** Investigation of the shoot length (**b**) ($n = 20$ independent seedlings), and seminal root length (**c**) ($n = 20$ independent seedlings) after one to seven days growth after germination (DAG). **d**–**f** Phenotypic comparison of the chilling tolerance (**d**), whole plant (**e**) and panicle length (**f**) between WT and *vig1a*. Scale bars, 4 cm (**d**), 15 cm (**e**) and 2 cm (**f**). The chilling tolerance for 14-day-old WT and *vig1a* was repeated three times with 80–96 seedlings per biological replicate and obtained similar results. The heading date for WT and *vig1a* plants was investigated three plots with 40–50 plants per plot. **g**–**j** Investigation of the survival rate (**g**) ($n = 3$ biologically independent experiments), heading date (**h**) ($n = 3$ biologically independent experiments), plant height (**i**) ($n = 30$ independent plants), and grain number per panicle (**j**) ($n = 30$ independent panicles). **k** Map-based cloning of gene *VIG1*. The black boxes indicate genes within the region between markers M5 and M6. The red box represents the candidate gene *OsbZIP01* (*LOC_Os01g07880*). The red letters indicate a guanine to adenine (G-A) point mutation occurred at the second exon of *OsbZIP01* in *vig1a*, which results in the 121st arginine to histidine (R-H) substitution of its encoding protein. **l** Seedling growth phenotype of WT and *vig1b*. Scale bars, 1 cm. **m, n** Investigation of the shoot length (**m**) ($n = 20$ independent seedlings), and seminal root length (**n**) ($n = 20$ independent seedlings) after one to seven days growth after germination (DAG). Values are the mean ± SD (two-tailed *t*-test, $^{***}P < 0.001$). Source data are provided as a Source Data file.

GNP, and that the *vig1a* mutant is not phenocopied by knocking out or overexpressing *OsbZIP01*.

Knocking out *OsbZIP18* or *OsbZIP48* show no obvious phenotypic alterations

VIG1 encodes a bZIP TF localized in the nucleus and the point mutation in *vig1a* maintained its subcellular localization (Supplementary Fig. 13a). To elucidate the possible mechanisms underlying the generation of *vig1a*, the homologous proteins of VIG1 in the rice genome were blasted. Nine paralogs were identified, with OsbZIP18 and OsbZIP48 exhibiting the closest relationship with VIG1 (Supplementary Fig. 13b). And the three bZIP TFs share highly similar protein structures, including a putative COP1 interacting domain in the N-terminal, a basic region at the center, and a leucine zipper region near the C-terminal region of VIG1 (Supplementary Fig. 13c). Moreover, all the three genes showed similar spatiotemporal expression profiles, with relatively higher expression being observed in both the flag leaf blade and leaf sheath (Supplementary Fig. 13d–f). It was noted that these three bZIP TFs are homologous proteins of *Arabidopsis* HY5 and HYH[32,33], which are interacting proteins. The three bZIP TFs also had remarkable similarities in their protein structure and expression patterns. For these reasons, their interactions were checked using the yeast two-hybrid (Y2H) assay and the results showed that each TF can interact with others (Fig. 3a). Furthermore, a bimolecular fluorescence complementation (BiFC) assay also confirmed the interactions of these TFs in rice protoplasts (Fig. 3b). The interaction between VIG1 and OsbZIP48 is consistent with the previous report[34]. Therefore, the interaction between VIG1 and OsbZIP18 was examined using the in vitro pull-down assay. The results revealed that only OsbZIP18-fused GST could interact with VIG1-fused MBP (Fig. 3c). Another truncated experiment in yeast revealed that 138–172 aa of VIG1 are responsible for its interaction with both OsbZIP18 and OsbZIP48 (Supplementary Fig. 14a, b). Moreover, the vig1a mutant protein maintained but vig1b lost the interaction with both OsbZIP18 and OsbZIP48 (Supplementary Fig. 14c–e).

Based on the close relationship with *VIG1*, the functions of *OsbZIP18* and *OsbZIP48* were identified. Target sites were designed at the first and third exons of *OsbZIP18*, respectively, and knocked it out in KY131 (Supplementary Fig. 15a; 16a). The resulting transgenic plants were identified as *OsbZIP18*-NK and *OsbZIP18*-CK, respectively. For *OsbZIP18*-NK, two homozygous lines with a 2-bp deletion (*OsbZIP18*-NK1) and a 4-bp deletion (*OsbZIP18*-NK2) in the coding region caused frameshift and truncated mutations of OsbZIP18 (Supplementary Fig. 17). The SV, CT, and GNP of the homozygous lines were comparable to the WT (Supplementary Fig. 15b–h). For *OsbZIP18*-CK, two homozygous lines with a 1-bp insertion (*OsbZIP18*-CK1) and a 3-bp deletion (*OsbZIP18*-CK2) in the coding region were identified. The former caused frameshift and truncated mutations of OsbZIP18, while the latter resulted in a 1-aa deletion and 1-aa substitution in the basic region of OsbZIP18 (Supplementary Fig. 18). Both lines showed no phenotypic differences compared to KY131 (Supplementary Fig. 16b–h). Similarly, target sites were also selected at the first and second exons of *OsbZIP48*, respectively, and knocked it out in KY131 (Supplementary Fig. 19a; 20a). The resulting materials were designated as *OsbZIP48*-NK and *OsbZIP48*-CK, respectively. And two homozygous lines of *OsbZIP48*-NK were identified, with a 1-bp deletion (*OsbZIP48*-NK1) and a 1-bp insertion (*OsbZIP48*-NK2) in the coding region (Supplementary Fig. 19a). Both lines caused frameshift and truncated mutations on OsbZIP48 (Supplementary Fig. 21), and showed no alterations in SV, CT, and GNP compared with KY131 (Supplementary Fig. 19b–h). For *OsbZIP48*-CK, two homozygous lines with a 1-bp insertion (*OsbZIP48*-CK1) and an 8-bp deletion (*OsbZIP48*-CK2) in the coding region were identified (Supplementary Fig. 20a). Both lines triggered frameshift and truncated mutations on OsbZIP48 (Supplementary Fig. 22), and showed no phenotypic changes, compared with the WT (Supplementary Fig. 20b–h). The results indicated the mutations that target genes *OsbZIP18* or *OsbZIP48* do not affect the SV, CT, and GNP, suggesting the overlapped functions between *VIG1*, *OsbZIP18*, and *OsbZIP48*.

vig1a is phenocopied by the simultaneous mutation of *VIG1* and *OsbZIP18*

To confirm the hypothesis that *VIG1*, *OsbZIP18*, and *OsbZIP48* have overlapped functions in regulating rice SV, CT, and GNP, a series of double and triple mutants were created by crossing *VIG1*-NK or *vig1b* with the different knockout lines of *OsbZIP18* and *OsbZIP48*. Unexpectedly, *VIG1*-NK*OsbZIP18*-NK (*1*-n*18*-n) and *VIG1*-NK*OsbZIP48*-NK (*1*-n*48*-n) double mutants, and *VIG1*-NK*OsbZIP18*-NK*OsbZIP48*-NK (*1*-n*18*-n*48*-n) triple mutants showed similar phenotypes in SV and CT, but GNP was lower compared to KY131 (Supplementary Fig. 23a–g). Surprisingly, the phenotype of *vig1bOsbZIP18*-CK (*1b18*-c) double mutants, including SV, CT, and GNP, resembled that of the *vig1a* mutant (Fig. 3d–j). However, the death rate among *1b18*-c double mutant plants was about a third of the total. These plants were also associated with delayed flowering time compared with *vig1a* (Fig. 3g). This indicated more severe defects caused by mutations on both *vig1b* and *OsbZIP18*-CK. Nevertheless, the phenotype of *vig1bOsbZIP18*-NK (*1b18*-n) double mutants resembled that of the *vig1b* mutant, while the phenotypes of *VIG1*-NK*OsbZIP18*-NK (*1*-n*18*-n) and *VIG1*-NK*OsbZIP18*-CK (*1*-n*18*-c) double mutants were similar to that of the *VIG1*-NK plants (Supplementary Fig. 24a–g). Given the obvious phenotypic differences between *1b18*-c and *1b18*-n double mutants, we deduced that *OsbZIP18* has alternative splicing and this was then confirmed by 5′ RACE (Supplementary Fig. 25a). The results showed that besides the 600 bp mRNA, another 411 bp isoform (designated as *OsbZIP18*-A1) was also identified and proved to encode a nuclear protein with 136 aa (Supplementary Fig. 25a, b). In addition, the interaction between vig1a and OsbZIP18-A1 was further confirmed using Y2H and BiFC assays (Supplementary Fig. 25c, d).

To further reveal the relationship between *VIG1* and *OsbZIP18*, the 600-bp full-length CDS of *OsbZIP18* was overexpressed in *vig1a* and the different lines (designated as *18*-OE) with up-regulated gene expression showed partially rescued SV, CT, and GNP, indicating that the functions of *OsbZIP18* overlapped with those of *VIG1* (Supplementary Fig. 26a–h). Based on these results, there is cooperative functionality between *OsbZIP18* and *VIG1*, and the point mutation in *vig1a* results in dysfunction of both *VIG1* and *OsbZIP18*.

https://doi.org/10.1038/s41467-024-52510-3

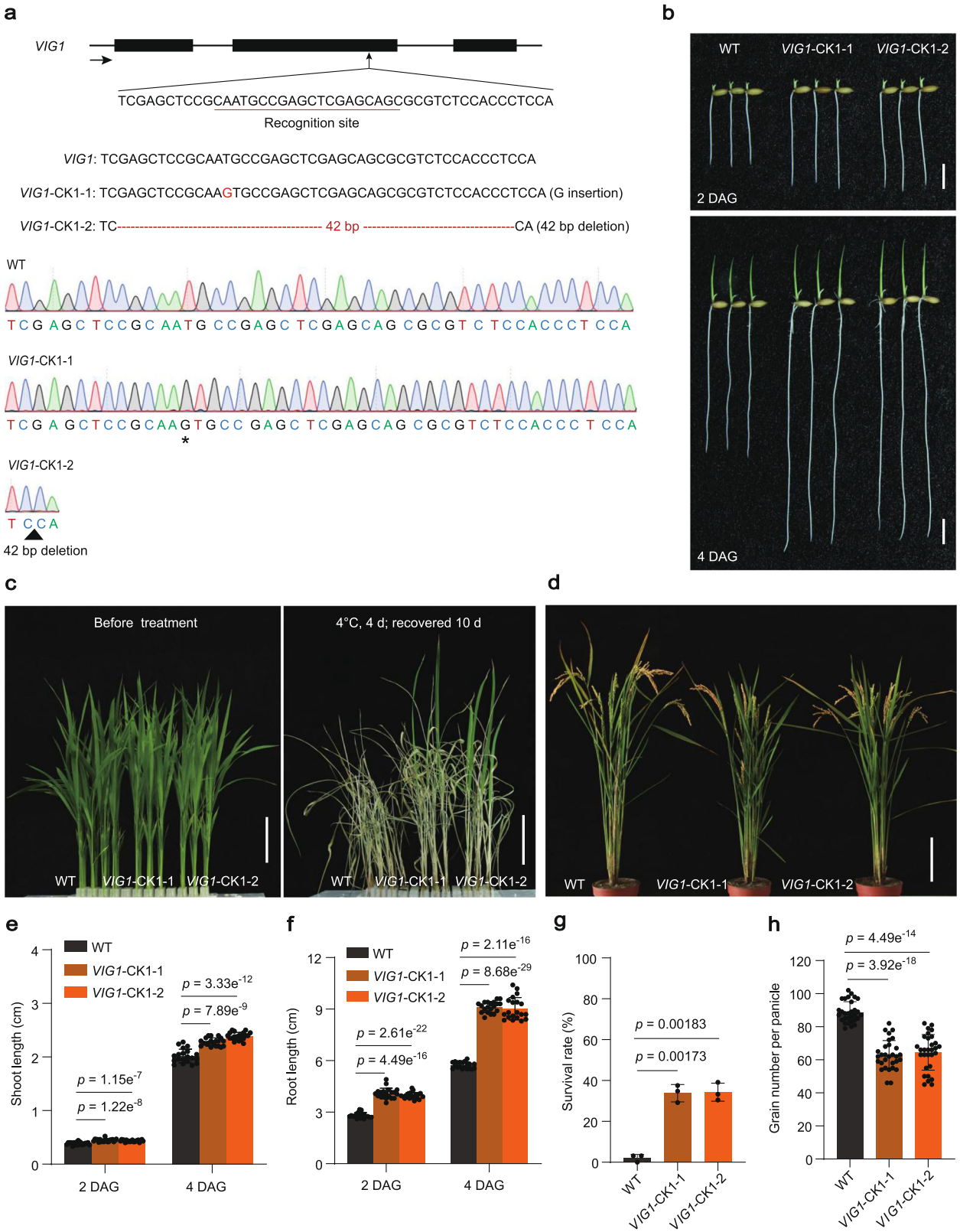

Fig. 2 | *VIG1*-CK lines showed increased seedling vigor and chilling tolerance, but decreased grain yield. a Schematic diagram of knocking out *VIG1* gene. The black boxes indicate the exons of *VIG1*. The black arrow indicates gene direction. The recognition site was underlined in red. The red letter and asterisk indicate inserted guanine, and the red dashed lines and black triangle indicate deleted 42 nucleotides, respectively. **b**–**d** The two- or four-day-old seedling phenotype (**b**), chilling tolerance (**c**), and whole plant (**d**) of WT and knock-out lines (*VIG1*-CK1-1 and *VIG1*-CK1-2). Scale bars, 1 cm (**b**), 4 cm (**c**) and 15 cm (**d**). The chilling tolerance for WT and *VIG1*-CK1 lines was repeated three times with 80–96 seedlings per biological replicate and obtained similar results. **e**–**h** Investigation of the shoot length (**e**) ($n = 20$ independent seedlings), seminal root length (**f**) ($n = 20$ independent seedlings), survival rate (**g**) ($n = 3$ biologically independent experiments), and grain number per panicle (**h**) ($n = 30$ independent panicles). Values are the mean ± SD (two-tailed *t*-test). Source data are provided as a Source Data file.

https://doi.org/10.1038/s41467-024-52510-3

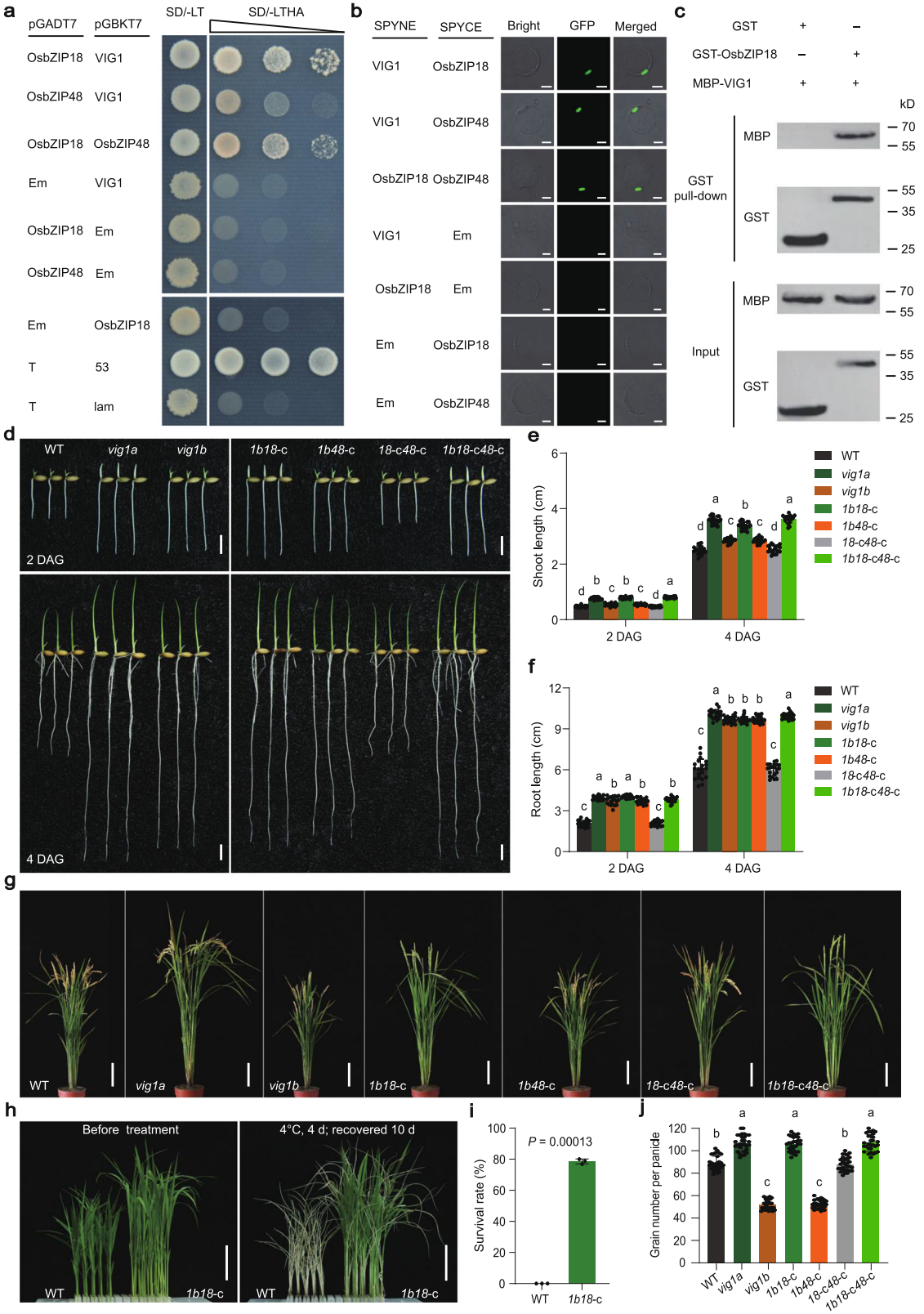

***vig1a* can be mimicked by mutations in the basic region of VIG1**

Considering that the arginine 121 to histidine (R121H) substitution in the basic region of VIG1 results in the *vig1a* phenotype, the function of this region required further verification. Therefore, arginine 121 was mutated to glycine (R121G), arginine 128 to proline (R128P), or the entire basic region was deleted without impairing other structures of VIG1. The resulting proteins were named vig1m1, vig1m2, and vig1m3, respectively (Supplementary Fig. 27a). Like vig1a, the mutant proteins still maintained nuclear localization (Supplementary Fig. 27b). All of them interacted with OsbZIP18 as confirmed using Y2H and BiFC assays (Supplementary Fig. 27c, d). This suggested that the mutant proteins and vig1a shared the same functions. Thus, corresponding genomic sequences of these three mutants were introduced into *vig1b* and transformation was conducted. Then, 26, 34, and 36 T_3

Fig. 3 | VIG1 regulates seedling vigor, chilling tolerance and grain number per panicle via the interaction with OsbZIP18. a The interaction between VIG1, OsbZIP18, and OsbZIP48 in the yeast. The combinations of pGBK-53 and pGADT7-T, pGBK-lam and pGADT7-T act as the positive and negative control, respectively. **b** The interaction of VIG1 with OsbZIP18 and OsbZIP48 was confirmed via BiFC. Scale bars, 10 μm. **c** The in vitro pull-down analysis of VIG1 with OsbZIP18. The experiments were repeated three times independently with similar results in (**a**–**c**). Em indicates the corresponding empty vectors in (**a, b**). **d**–**f** The seedling phenotype of two- or four-day-old WT, *vig1a*, *vig1b*, *vig1bOsbZIP18*-CK (*1b18*-c), *vig1-bOsbZIP48*-CK (*1b48*-c), *OsbZIP18*-CK*OsbZIP48*-CK (*18-c48*-c), and *vig1bOsbZIP18*-CK*OsbZIP48*-CK (*1b18-c48*-c) plants (**d**) and investigation of the shoot length (**e**) ($n = 20$ independent seedlings), and seminal root length (**f**) ($n = 20$ independent seedlings). Scale bars, 1 cm (**d**). **g** The phenotype of the whole plant of WT, *vig1a*, *vig1b*, *1b18*-c, *1b48*-c, *18-c48*-c, and *1b18-c48*-c at the mature stage of WT. Scale bars, 15 cm. **h** The phenotype of WT and *1b18*-c double mutants before and after chilling stress treatment. Scale bars, 4 cm. The chilling tolerance for WT and *1b18*-c plants was repeated three times with 80–96 seedlings per biological replicate and obtained similar results. **i, j** Investigation of the survival rate (**i**) ($n = 3$ biologically independent experiments), and grain number per panicle (**j**) ($n = 30$ independent panicles). Values are the mean ± SD. Statistical significance was determined by one-way ANOVA with Tukey's multiple comparisons test, different letters represent significant differences at 5% in (**e, f, j**), and the significant difference was determined by two-tailed Student's *t*-test in (**i**). Source data are provided as a Source Data file.

complementary lines were obtained, respectively. All the lines for each mutant fully resembled the phenotypes of *vig1a*, including SV, CT, and GNP (Supplementary Fig. 27e–g; 28; 29), indicating that mutations in the basic region of VIG1, besides the point mutation in *vig1a*, are capable of retaining the *vig1a* phenotype.

Considering that R121H substitution in vig1a does not affect its interaction with OsbZIP18, a knockout target was designed in the leucine zipper region (138-172 aa) of VIG1 which is responsible for the interaction with OsbZIP18, and conducted transgene in the *vig1a* background (Fig. 4a). Two homozygous lines with a 1-bp insertion (*VIG1*-CK1^{vig1a}) and a 21-bp deletion (*VIG1*-CK2^{vig1a}), were selected for phenotypic analysis (Fig. 4a). Both strains showed disruption of the leucine zipper region of vig1a (Supplementary Fig. 30) and presented phenotypes similar to *vig1b* including SV and GNP (Fig. 4b, d, e, f, h). In addition, the CT of the *VIG1*-CK^{vig1a} lines significantly decreased compared with that for *vig1a* (Fig. 4c, g), suggesting that the disruption of the interacting domain in *vig1a* causes the phenotypic conversion of *vig1a* to *vig1b*. The results showed that besides the point mutation, the generation of *vig1a* also relies on the interaction between vig1a and OsbZIP18.

VIG1 regulates SV and CT through different downstream genes

To elucidate the detail mechanisms underlying the regulation of SV, CT, and GNP by *VIG1*, the RNA sequencing analyses were conducted by taking the shoots of seven-day-old seedlings of KY131, *vig1a*, and *vig1b*. The transcriptome data showed that a total of 1268 genes were differentially expressed (at least two-fold change in the expression, 5% significant difference) in *vig1a* compared to the wild-type, of which 892 genes were up-regulated and 376 genes down-regulated (Fig. 5a). Additionally, a total of 595 genes were differentially expressed in *vig1b*, with 435 of them being up-regulated and 160 down-regulated (Fig. 5a). Among the differentially expressed genes, 338 were co-regulated in both mutants (Fig. 5b).

Considering that tissue growth is closely related to cell division and elongation, while elevated CT tightly correlates with the expression of cold-tolerant genes. The transcriptome data revealed that 15 cell division and cell expansion genes, and six *OsDREBs* cold tolerance genes were significantly up-regulated in *vig1a* (Supplementary Fig. 31a). On the other hand, five cell division and cell expansion genes, and five *OsDREBs* cold-tolerant genes were significantly up-regulated in *vig1b* (Supplementary Fig. 31b). The abundance of genes associated with cell division, cell expansion, and CT were lower in *vig1b* than in *vig1a* (Supplementary Fig. 31a, b). This is consistent with our previous results, which showed that the shoot length and CT of *vig1a* were significantly better than those for *vig1b* (Fig. 3d, e; Supplementary Fig. 6b, g). Therefore, cell expansion, cell division, and *OsDREBs* genes may be responsible for *VIG1*-mediated shoot elongation and CT.

Thus, nine up-regulated genes with relatively higher expression levels were selected from *vig1a* for further verification (Supplementary Fig. 31a, c). Consistently, our real-time PCR showed that all the selected genes were up-regulated in the seven-day-old shoots of *vig1a*, and genes *EXPB4*, *EXLA2*, *CYCD1-2*, *OsDREB1A*, and *OsDREB1B* presented relatively higher expression levels (Supplementary Fig. 31c). Thus, the transcripts of these five genes were also checked in the seven-day-old shoots of *vig1b*, *VIG1*-NK, *VIG1*-CK, and *VIG1*-OE. Consistent with our phenotypic results, increased expression levels in both *vig1b* and *VIG1*-CK were observed for genes *EXPB4*, *OsDREB1A*, and *OsDREB1B*. However, an opposite tendency was observed in *VIG1*-OE (Supplementary Fig. 31f). And all five genes showed comparable expression levels in *VIG1*-NK than in the wide-type (Supplementary Fig. 31f). It's also important to note that the expression levels of genes *EXLA2* and *CYCD1-2* remained unchanged in *vig1b*, *VIG1*-NK, *VIG1*-CK, and *VIG1*-OE (Supplementary Fig. 31f). Moreover, the expression levels of *OsDREB1A* and *OsDREB1B* were significantly higher in the 14-day-old shoots of *vig1a* than in the WT, before and after cold stress treatment (Supplementary Fig. 31d, e). These results suggest that *VIG1* regulates SV and CT by modulating cell expansion, cell division, and cold-tolerant genes.

VIG1 functions with OsbZIP18 in regulating downstream targets

Ehd1 is one of the targets of OsbZIP01 (also known as OsRE1) and has been reported for its positive regulatory role in rice heading date and its opposite effects in GNP[35,36]. Thus, transcripts of *Ehd1* were checked in various materials of *VIG1*. Observations showed that *Ehd1* was significantly higher in *VIG1*-NK, *vig1b*, and *VIG1*-CK plants, but remarkably lower in *VIG1*-OE lines (Supplementary Fig. 32a), which is consistent with our phenotypic results that showed that *VIG1*-NK, *vig1b*, and *VIG1*-CK materials produce lower GNP while *VIG1*-OE flowers late and generates higher GNP. To further confirm these results, a target site was designed at the first exon of *Ehd1*, and knocked it out in *vig1b* (Supplementary Fig. 32c). Two homozygous lines of *Ehd1* with a 1-bp insertion (*Ehd1*-KO1^{vig1b}) and a 2-bp deletion (*Ehd1*-KO2^{vig1b}) in the coding region were identified (Supplementary Fig. 32c). Both lines resulted in frameshift mutations of Ehd1 (Supplementary Fig. 33), and exhibited a 15- or 16-day delay in flowering than *vig1b* (Supplementary Fig. 32d, e). In addition, *Ehd1*-KO^{vig1b} lines presented markedly increased plant height, GNP, and grain yield per plant (GYP) than *vig1b* (Supplementary Fig. 32d, g, h, j). However, the tiller number and seed setting rate remained unchanged (Supplementary Fig. 32f, i). These results indicate that the up-regulated expression of *Ehd1* was responsible for the decreased grain yield in *VIG1*-NK, *vig1b*, and *VIG1*-CK plants, while its suppression caused the opposite trends in *VIG1*-OE lines.

However, the transcript of *Ehd1* in *vig1a* remained identical to that of in KY131 (Supplementary Fig. 32a). Moreover, results from the Luciferase (LUC) assay revealed that vig1a had a comparable repression effect on *Ehd1* (Supplementary Fig. 32b), suggesting that *Ehd1* is not responsible for the enhanced GNP in *vig1a*. Therefore, the transcriptome data was further analyzed, and remarkably enhanced expression of *OsPID* was noted, only in *vig1a*. *OsPID* was reported to positively regulate rice GNP[37]. Thus, the elevated expression of *OsPID* in *vig1a* was further confirmed in 1–2 mm young panicles using real-time PCR (Supplementary Fig. 32a). However, no significant changes on the *OsPID* transcript

https://doi.org/10.1038/s41467-024-52510-3

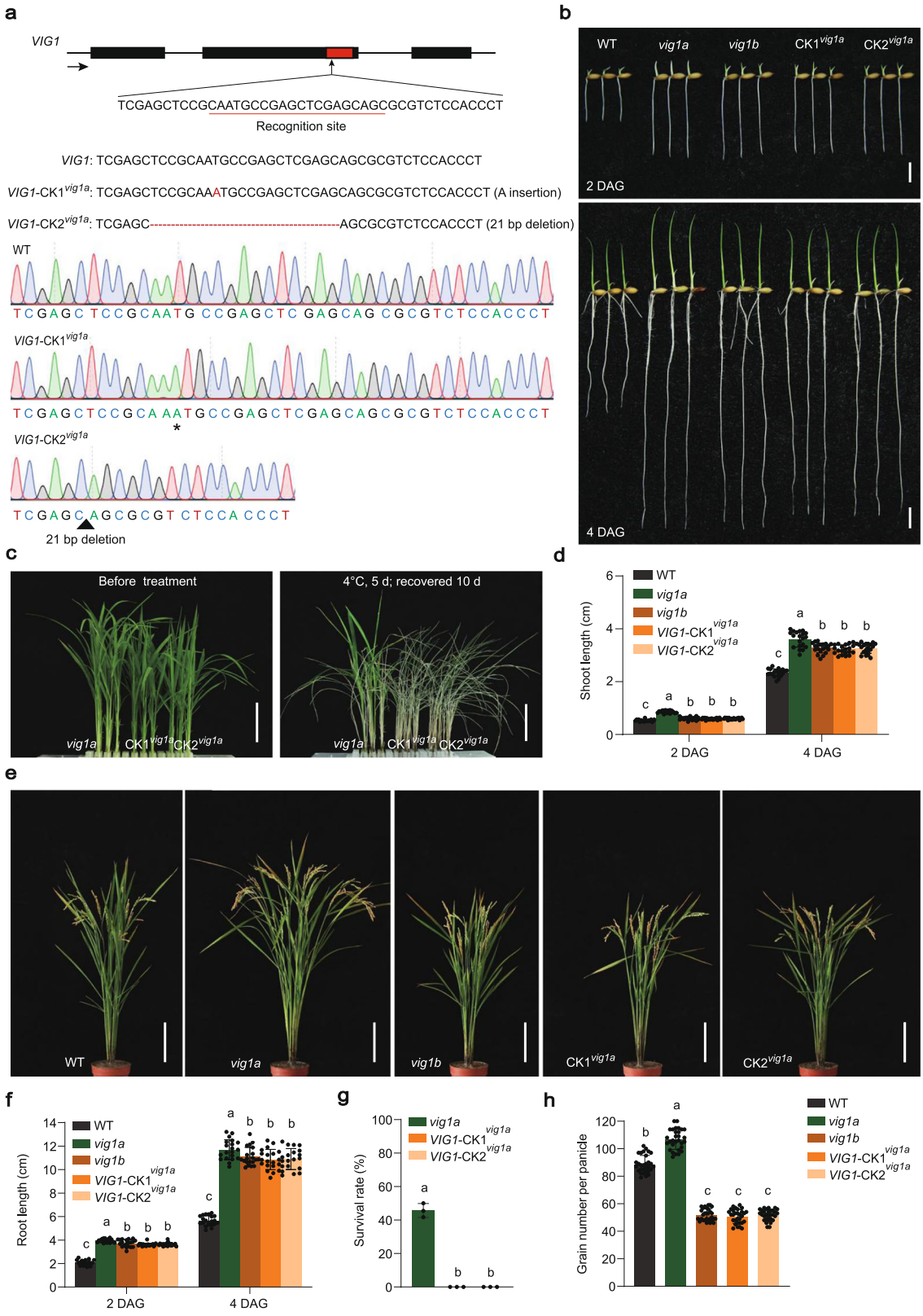

were observed in other materials (Supplementary Fig. 32a), suggesting the synergistical regulation of *OsPID* by VIG1 and OsbZIP18.

Considering that the transcripts of genes *EXPB4*, *EXLA2*, *CYCD1-2*, *OsDREB1A*, *OsDREB1B*, and *OsPID* correlate well with our phenotypic results, further experiments were conducted to verify the binding between VIG1 and the potential targets. The bZIP TF OsbZIP01/VIG1 was formerly demonstrated to preferentially bind to the A-box (TACGTA), G-box (GACGTC), or C-box (CACGTG) in the promoters of target genes[35,38]. Therefore, putative binding sites were examined and single or multiple A-, G- or C-boxes were identified in the 2.0-kb promoters and 3′-UTR regions of different potential targets (Fig. 5d). The results from LUC assays showed that VIG1 directly bound to the promoters of genes *EXPB4* and *OsPID*, but OsbZIP18 bound to genes *EXLA2*, *CYCD1-2*,

Fig. 4 | The generation of *vig1a* relies on the interaction between vig1a and OsbZIP18. a Schematic diagram of knocking out *vig1a* in the leucine zipper region (*VIG1*-CK^{vig1a}). The black boxes indicate the exons of *VIG1*. The black arrow indicates gene direction. The red box indicates gene sequences encoding the leucine zipper region of VIG1. The recognition site was underlined in red. The red letter and asterisk indicate inserted adenine, and the red dashed lines and black triangle indicate deleted 21 nucleotides, respectively. **b** The phenotype of two- or four-day-old WT, *vig1a*, *vig1b*, and *VIG1*-CK^{vig1a} (CK^{vig1a}) seedlings. Scale bars, 1 cm. **c** The phenotype of *vig1a* and CK^{vig1a} seedlings before and after chilling stress treatment. Scale bars, 4 cm. The chilling tolerance for *vig1a* and CK^{vig1a} plants was repeated three times with 80-96 seedlings per biological replicate and obtained similar results. **d** Investigation of the shoot length. Values are the mean ± SD ($n = 20$ independent seedlings). **e** The phenotype of the whole plant of WT, *vig1a*, *vig1b*, and CK^{vig1a} at the mature stage. Scale bars, 15 cm. **f**–**h** Investigation of the root length (**f**) ($n = 20$ independent seedlings), survival rate (**g**) ($n = 3$ biologically independent experiments), and grain number per panicle (**h**) ($n = 30$ independent panicles). Values are the mean ± SD. Statistical significance was determined by one-way ANOVA with Tukey's multiple comparisons test, different letters represent significant differences at 5%. Source data are provided as a Source Data file.

OsDREB1A, *OsDREB1B*, and *OsPID* promoters (Fig. 5c–e). Similarly, both VIG1 and OsbZIP18 repressed the expression of their downstream targets (Fig. 5c–e). Using the yeast-one hybrid (Y1H) system, the binding of VIG1 and OsbZIP18 with their respective targets was further confirmed (Fig. 5f; Supplementary Fig. 34a). In contrast, both VIG1 and OsbZIP18 failed to bind to the mutated motif of their downstream genes (Fig. 5f; Supplementary Fig. 34a). The electrophoretic mobility shift assays (EMSA) also confirmed the direct binding of VIG1 and OsbZIP18 with the *cis*-element of their targets. Consistently, VIG1 showed direct binding to hot probes of genes *EXPB4* and *OsPID*, and OsbZIP18 bound to the hot probes of genes *EXLA2, CYCD1-2, OsDREB1A, OsDREB1B, and OsPID* (Fig. 5g; Supplementary Fig. 34b). Both two proteins failed to bind to the mutated probes of their target genes (Fig. 5g; Supplementary Fig. 34b), indicating that VIG1 cooperates with OsbZIP18 in balancing SV, CT, and GNP.

vig1a shows great potential in improving SV, CT, and GNP in *Indica* rice

Based on the remarkable performance of *vig1a* in enhancing SV, CT, and GNP in *Japonica* rice, we repeatedly backcrossed *vig1a* with ZF802 (*Indica*), and constructed near-isogenic lines (Fig. 6a). Compared with ZF802, NIL-*vig1a* showed markedly increased SV, with the shoot and root length being significantly longer (Fig. 6b–d). In addition, NIL-*vig1a* presented significantly higher survival rates after being exposed to chilling stress treatment for three days (Fig. 6b, e). Moreover, the plant height, GNP, and GYP were better for NIL-*vig1a* than ZF802 (Fig. 6b, f–h), indicating a great potential of *vig1a* in improving SV, CT, and GNP in *Indica* rice.

Discussion

Previous studies uncovered the vital roles that *VIG1* (*OsbZIP01*) plays in regulating the flowering time[35], root development[39], photomorphogenesis[34], and grain yield[40] of rice plants. Of which, OsbZIP01 (OsRE1) acts as a minor heading date regulator by interacting with OsRIP1 to suppress the expression of *Ehd1*, a well-known target in heading date and GNP[35,41]. The mutation of OsbZIP1/OUR1 promotes root development, which could be attributed to the suppression of auxin signaling[39]. Moreover, it was revealed that *OsbZIP01* positively regulates photomorphogenesis, and two splices of this gene play divergent roles in mediating seedling development in light and dark environments, respectively[34]. Under low nitrogen and phosphorus conditions, enhanced root length was reported for *88n*[40], which is a mutant of *OsbZIP01*. Improved yield was also noted, mainly attributed to the increased Pi uptake (PUpE) and nitrogen use efficiency (NUtE)[40]. Even though the function of OsbZIP01 in different traits of rice has been investigated and reported, little is known about its role in rice SV, CT, and GNP.

SV, CT, and GNP are three important agronomic traits that determine rice growth, development, and tolerance to adverse environments. For each trait, many regulators have been elucidated[17,18,26,27,42–46]. Among them, *OsMADS25* and *OsPAO5* are vital genes that regulate seedling development[43,44], while *OsDREBs*, *COLD1*, and *OsbZIP73* play significant roles in CT in rice seedlings[17,18,45]. And *Gn1a*, *DEP1*, *GNP1*, and *FZP* are the important regulators of rice GNP[26,27,42,46]. However, up to now, only gene *IPA1* has been revealed to simultaneously regulate SV, CT, and GNP[28–30,47]. *IPA1* promotes CT and GNP, but represses SV[28–30], suggesting a trade-off role of *IPA1* as far as the regulation of SV, CT, and GNP is concerned. The results from this study show that *vig1a* simultaneously enhances SV, CT, and GNP through the coordinative roles of VIG1 and OsbZIP18 in repressing the expression of cell expansion and cell division genes, *OsDREBs*, and *OsPID* (Fig. 1a–j; 5c–g; Supplementary Fig. 31), indicating a great potential of *VIG1* in simultaneously improving SV, CT, and GNP.

However, when *VIG1* was genome-edited through the CRISPR-Cas9 system, the SV and CT of *VIG1*-NK were comparable to that of the WT (Supplementary Fig. 7a–c, e–g). On the other hand, *VIG1*-CK presented significantly enhanced root length (Fig. 2b, f), and this was consistent with reports from other studies[39]. Elevated CT was also noted for *VIG1*-CK (Fig. 2c, g). Given that *OsbZIP1* showed alternative splicing, generating the 612-bp and 345-bp splices, respectively[34]. This suggests the contribution of different splices in the phenotypic divergence of *VIG1*-NK and *VIG1*-CK. Thus, both splices were examined in *VIG1*-NK and *VIG1*-CK through 5′ RACE. The findings showed that two of the *VIG1* splices were destroyed in *VIG1*-CK and *vig1b*, but the 345-bp mRNA remained completely reserved in *VIG1*-NK (Supplementary Figs. 35–39). This implies that the two splices of *VIG1* play different roles in rice development. The 612-bp splice is responsible for grain yield control, and both the 612-bp and 345-bp splices exhibit redundant functionality in SV and CT. When *VIG1* was overexpressed, the transgenic lines showed remarkably decreased shoot lengths and CT compared to the *VIG1*-CK. However, the root lengths were significantly increased, possibly due to the complex hormonal balance that existed in the roots.

Except for SV and CT, both *VIG1*-NK and *VIG1*-CK showed remarkably reduced GNP, whereas *VIG1*-OE exhibited late flowering and enhanced grain production, consistent with the previous report that OsbZIP01 acts as the repressor of *Ehd1* (Fig. 2d, h; Supplementary Figs. 7d, h and 12g, j), a target that promotes heading but suppresses GNP[35,36,41]. However, no obvious phenotype associated with early flowering was observed in *VIG1*-NK, *vig1b*, or *VIG1*-CK, compared with WT. These discrepancies could be due to the background differences. In addition, compared to the WT, *vig1a* also flowered late and produced more grains (Fig. 1f, h, j; Supplementary Fig. 1d). The data from this study showed that elevated expression of *OsPID* was responsible for the increased grain number associated with *vig1a* (Supplementary Fig. 32a). However, overexpression of *OsPID* doesn't alter the rice flowering time[37], so the late flowering of *vig1a* is not caused by the up-regulation of *OsPID*. *OsbZIP01* was previously reported to act as a positive regulator of photomorphogenesis, where incident light determines growth patterns[34]. However, no significant photomorphogenic defects were observed in *VIG1*-NK, *vig1b*, and *VIG1*-CK (Figs. 1l, 2b; Supplementary Fig. 7b), though the *vig1a* seedlings, as well as the *1b18*-c double and *1b18-c48*-c triple mutants showed markedly elongated coleoptiles and subsequent late flowering (Figs. 1a, 3d; Supplementary Fig. 1a, d). Moreover, the late flowering phenotype of *vig1a* was rescued when *OsbZIP18* was overexpressed. This suggests that simultaneous dysfunction in both *VIG1* and *OsbZIP18* is responsible for the decreased photosensitivity and subsequent late flowering associated with *vig1a*.

https://doi.org/10.1038/s41467-024-52510-3

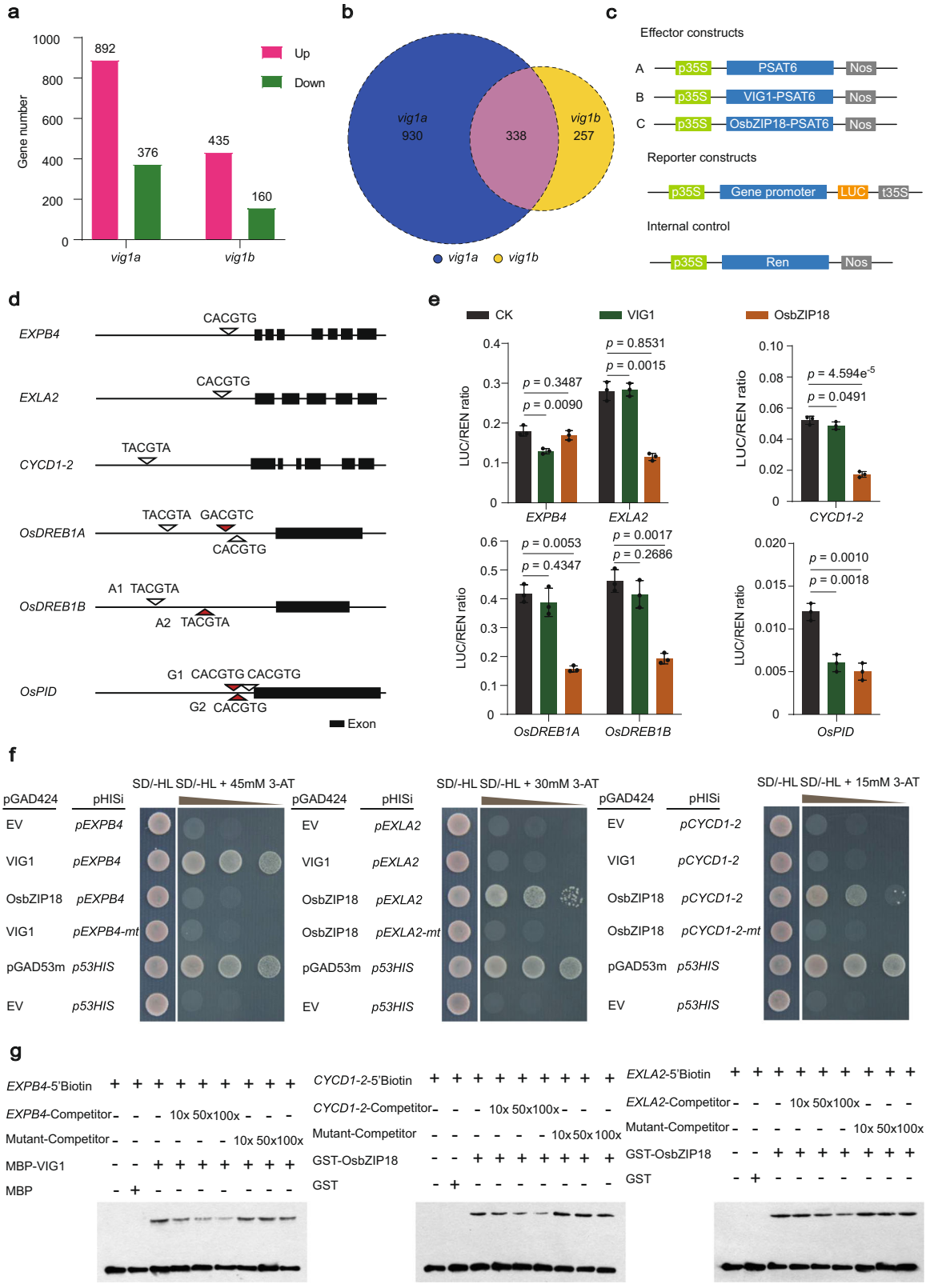

VIG1 encodes a bZIP TF that is homologous to *Arabidopsis* HY5, which has crucial roles in plant development and stress tolerance. *HY5* promotes photomorphogenesis and positively regulates cold acclimation in *Arabidopsis*[32,48]. In this study, the role of *VIG1* in negatively regulating shoot length and CT is revealed, suggesting functional divergence of *HY5* between monocot and dicot plants. *HYH*, a homolog of *Arabidopsis HY5*, also plays an important role in blue light mediated photomorphogenesis, and the mutation of *HYH* augments the hypocotyl length of *hy5*[33]. Similarly, in the rice genome, *OsbZIP01*/*VIG1*, *OsbZIP18*, and *OsbZIP48* are identified as the homologs of *Arabidopsis HY5* and *HYH*. The mutation of *OsbZIP18*-CK also aggravates the traits of *vig1b*, including SV, CT, and GNP (Fig. 3d–j). In addition, the single mutation of *OsbZIP18* showed no phenotypic differences compared to the WT (Supplementary Figs. 15, 16), which is consistent with the

Fig. 5 | VIG1 functions with OsbZIP18 in repressing downstream genes connected with cell expansion, cell division, chilling tolerance, and grain number per panicle. a A total of 1268 and 595 DEGs were identified in *vig1a* and *vig1b*, respectively. **b** A total of 338 DEGs (indicated by the pink color) were found co-regulated in both *vig1a* and *vig1b*. **c**–**g** Analysis of the binding of VIG1 and OsbZIP18 to target gene promoters using the luciferase reporter (LUC) system, yeast one-hybrid (Y1H), and electrophoretic mobility shift assays (EMSA). **c** Schematic diagram of the constructs used for transactivation activity assay. **d** Scanning of the VIG1 binding motif 'C/T/GACGTG/A/C' across the promoter region of genes downregulated in *vig1a*. The length of promoter sequence is 2 kb for each gene. **e** Transcriptional repression of VIG1 and OsbZIP18 on downstream targets. Values are the mean ± SD ($n = 3$ biological replicates, two-tailed *t*-tests). **f, g** VIG1 directly binds to the promoter of *EXPB4*, while OsbZIP18 binds to the promoter of *EXLA2* and *CYCD1-2* which are confirmed by Y1H (**f**) and EMSA (**g**). The pGAD53m-*p53HIS* and pGAD424-*p53HIS* combinations are taken as the positive and negative controls, respectively, in the Y1H assays. The experiments in (**f, g**) are repeated at least three times with similar results. Source data are provided as a Source Data file.

previous report[49]. In a former report, impairment of the *OsbZIP48* function caused seedling-lethal phenotypes[50]. However, in our study, the single mutation of *OsbZIP48* also presented a phenotype comparable with that of WT (Supplementary Figs. 19, 20). The possible explanation for this finding is background differences.

In addition, the phenotype shown by *vig1a* was similar to that of the *1b18*-c double mutant. This could be because that the *vig1a* allele has a negative activity toward OsbZIP01 and OsbZIP48 proteins. A similar genetic phenomenon was also revealed in *DA1*- and *DAR1*-mediated seed and organ size development in *Arabidopsis*[51]. And the results from this study showed that the special genetic phenomenon between vig1a and OsbZIP18 relies on the physical interactions of these two. Once the interaction is destroyed, the phenotype of *vig1a* will change to that of the *vig1b* (Fig. 4). This suggests that *OsbZIP18* and *VIG1* exhibit overlapped function, as proven by the overexpression of *OsbZIP18* in the *vig1a* background (Supplementary Fig. 26). The mutations in the basic region of VIG1, besides the point mutation in *vig1a*, present similar effects on OsbZIP18 (Supplementary Figs. 27–29), indicating that the basic region of VIG1 plays an important regulatory role. Nevertheless, such a regulatory mechanism has not been observed for *Arabidopsis* HY5, indicating that a more complicated role of VIG1 in monocot plants.

The point mutation in *vig1a* results in dysfunction of both OsbZIP01 and OsbZIP18 proteins. A clear understanding of how vig1a impacts the function of OsbZIP18 requires a detail analysis of both the spatial and structural characteristics of vig1a and OsbZIP18. Genetically, except for the mutations in *vig1m1*, *vig1m2* and *vig1m3*, whether other point mutations, insertions, or deletions in the basic region of OsbZIP01 will generate the *vig1a* phenotype remain to be explored.

In summary, this study shows that VIG1 synergistically represses cell expansion, cell division, *OsDREBs*, *OsPID*, and *Ehd1* genes by interacting with OsbZIP18 through the leucine zipper region, which triggers a complicated balance in SV, CT, and GNP traits of rice (Fig. 7). Additionally, the findings showed that *vig1a* enhances SV, CT, and GNP, in both *Japonica* and *Indica* rice, and the mutations in the basic region of VIG1 also retain the *vig1a* phenotype. These results suggest that *vig1a* is a target in rice paddy-direct seeding.

Methods

Plant materials and growth conditions

The *vig1a* and *vig1b* mutant were screened from the NaN_3-mutagenized M_2 population of KY131 (*japonica*). The near isogenic line of *vig1a* (NIL-*vig1a*) (BC_4F_3) was constructed by repeatedly backcrossing *vig1a* with ZF802 (*indica*) and conducted background selection before each backcross to exclude the noise. Primers used for NIL construction and background selection are listed in Supplementary Data 1, which also can be referred to Xu et al.[52]. All the materials used in this study were grown in the experimental stations of the Institute of Genetics and Developmental Biology in Changping (40.2°_N/116.2°_E), Beijing during the summer or Lingshui (18.5°_N, 110.0°_E), Hainan province during the winter.

For seedling culture, healthy seeds were surface-sterilized with 3% sodium hypochlorite for 30 min, soaked at 37 °C for 3 d. Germinating seeds with shoot length of 2 mm were selected and sown onto an incubating net with foam, and water-cultured in the phytotron (SANYO) with 12 h light (28 °C)/12 h dark (28 °C), 65-70% relative humidity, and 150 μM m^{-2} s^{-1} photon flux density. Morphological investigation was performed different days after incubation.

For chilling tolerance, healthy seeds were surface-sterilized with 3% sodium hypochlorite for 30 min, soaked at 37 °C for 3 d. Germinating seeds were sown into 96-well PCR plates, and water-cultured in the phytotron (SANYO) with 12 h light (28 °C)/12 h dark (28 °C), 65–70% relative humidity and 150 μM m^{-2} s^{-1} photon flux density. Five-day-old pre-cultured seedlings were then transferred to outdoor natural conditions for further growth until 14-day-old. The resulting seedlings were treated at 4 °C for different days in the above-mentioned phytotron (SANYO), and then recovered under normal conditions (28 °C, 12 h light /12 h dark). Survival rate was calculated as the percentage of the number of seedlings with green leaves to the total number of treated seedlings.

Cloning of *VIG1*

For cloning of *VIG1*, *vig1a* was crossed with the *japonica* variety KD8 to construct the mapping population. Whole genome polymorphic markers were designed based on resequencing data of the two parents (30×), and molecular markers used for mapping are listed in Supplementary Data 1. Using 20 bulked F_2 plants with WT and mutant phenotypes respectively, the candidate gene was initially mapped to the short arm of chromosome 1 between the markers M1 and M2. Further analysis of the F_2 mutant plants subsequently fine-mapped the causal gene to the region between the markers M5 and M6, and sequence comparison was then performed between *vig1a* and WT based on the resequencing data (30×). A single-nucleotide substitution (G-A) at the second exon of gene *LOC_Os01g07880* was identified in the *vig1a* mutant, leading to the R121H substitution in the basic region of VIG1 in the mutant.

Morphological investigation and histological analysis

Investigation of agronomic traits was performed on plant height and grain number per main panicle for different materials at the mature stage. Each trait was investigated for at least 20 individual plants. Investigation of days to heading was performed for materials sown at the same time and grown in the identical field conditions in Changping (40.2°_N/116.2°_E), Beijing during the summer.

For histological analysis, coleoptiles from four-day-old shoots of WT and *vig1a* were detached and fixed in 2.5% glutaraldehyde (with 1 mL of 25% glutaraldehyde, 4 mL of ddH_2O, and 5 mL of 0.2 M phosphate buffer) overnight at 4 °C after 20 min vacuum treatment. After dehydration with a gradient of ethanol, samples were then dehydrated in a Critical point dryer (Leica EM CPD300). For SEM observation, the inner side of coleoptiles were unfolded, sprayed with gold particles in a vacuum with an ion sputtering device (JFC-1100E, JEOL, Tokyo, Japan) and scanned with a scanning electron microscope (S-3000N, Hitachi, Japan). The cell size was measured with the Image J software (https://imagej.net/ij/download.html).

Vector construction and transformation

To complement *vig1a* with WT sequence, a 3.52 kb genomic fragment (containing the entire coding region, 2198 bp upstream of ATG and 542 bp downstream of TAG) was amplified from WT, and cloned into the pZH2B vector through enzyme digestion and ligation.

https://doi.org/10.1038/s41467-024-52510-3

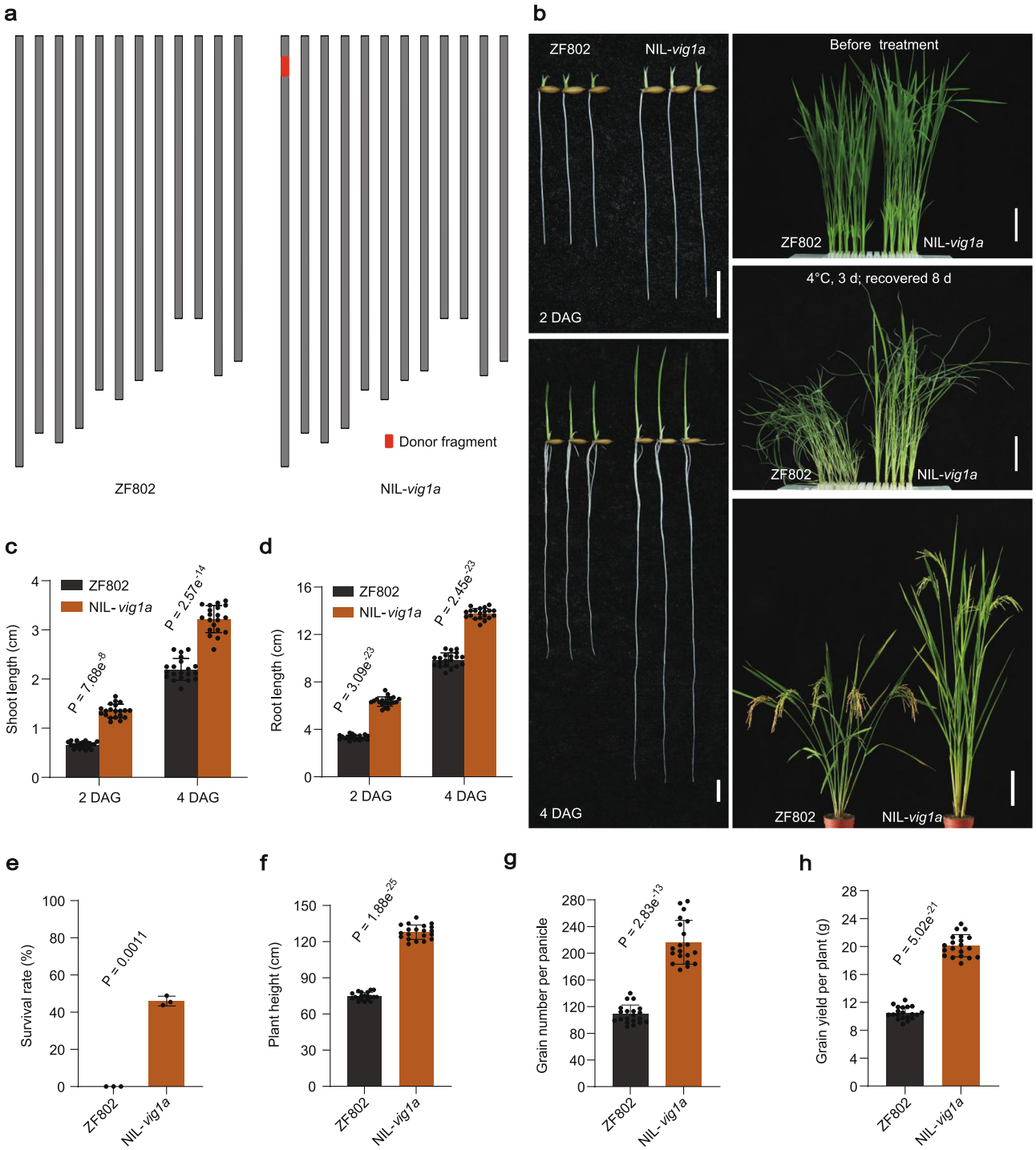

Fig. 6 | NIL-*vig1a* shows elevated seedling vigor, chilling tolerance, and grain yield. a Schematic diagram of the chromosomes. The donor fragment is shown in red. **b** Phenotype of the seedling vigor, chilling tolerance, and whole plant for ZF802 and NIL-*vig1a*. Scale bars, 1 cm left (**b**), 4 cm upper and middle right (**b**), and 15 cm bottom right (**b**). **c**–**h** Investigation of the shoot length (**c**) ($n = 20$ independent seedlings), seminal root length (**d**) ($n = 20$ independent seedlings), survival rate (**e**) ($n = 3$ biologically independent experiments), plant height (**f**) ($n = 20$ independent plants), grain number per panicle (**g**) ($n = 20$ independent panicles), and grain yield per plant (**h**) ($n = 20$ independent plants). Values are the mean ± SD (two-tailed *t*-test). The chilling tolerance for ZF802 and NIL-*vig1a* was repeated three times with 80-160 seedlings per biological replicate and obtained similar results. Source data are provided as a Source Data file.

To complement *vig1b* with WT or *vig1a* sequence, a 3.52 kb genomic fragment (containing the entire coding region, 2198 bp upstream of ATG and 542 bp downstream of TAG) was amplified from WT or *vig1a*, respectively, and cloned into the pZH2B vector through enzyme digestion and ligation.

To complement *vig1b* with VIG1 basic region modified sequence, the aforementioned 3.52 kb genomic fragment from WT was used to create nucleotide substitutions or deletions through manipulation of the primers, respectively, and the resulting fragments were cloned into the pZH2B vector by enzyme digestion and ligation.

https://doi.org/10.1038/s41467-024-52510-3

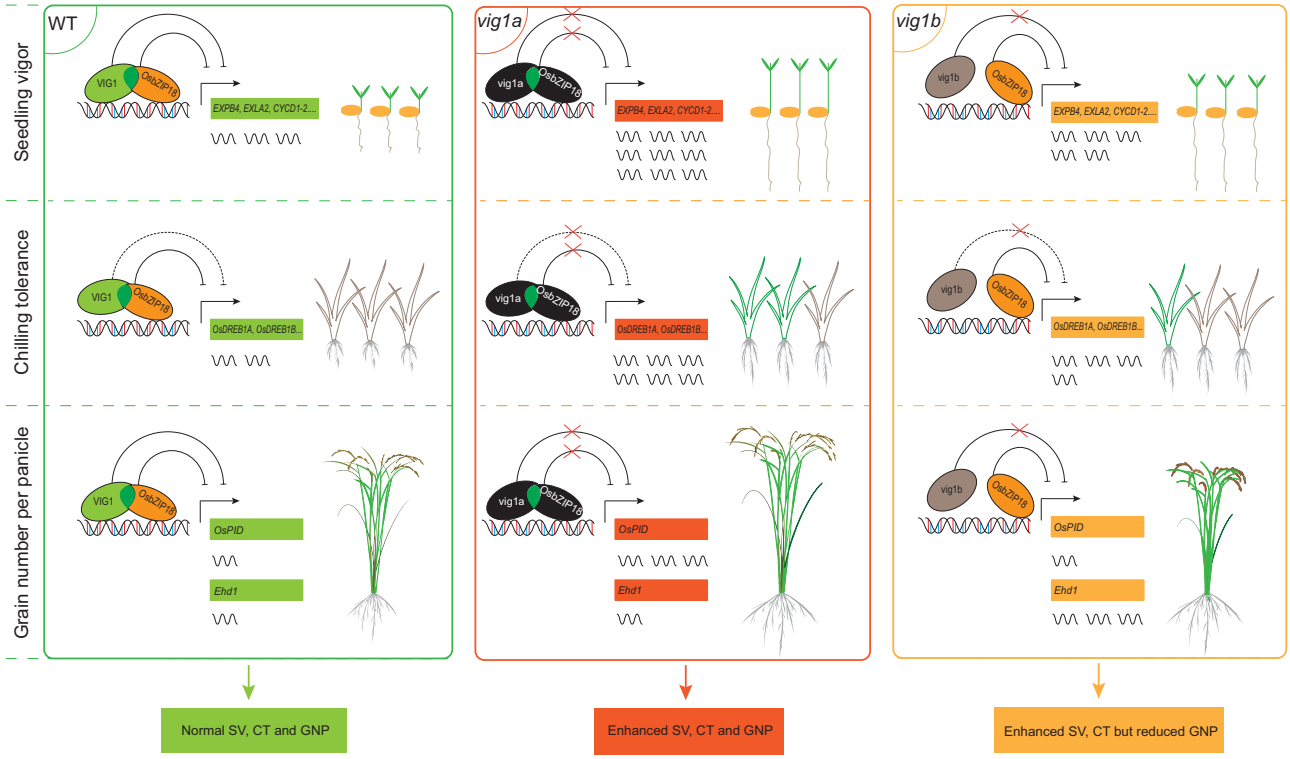

Fig. 7 | A working model of VIG1 and OsbZIP18 mediated seedling vigor, chilling tolerance, and grain number per panicle. VIG1 interacts with OsbZIP18 via the leucine zipper region (ZIP), and two proteins function synergistically in repressing the transcription of downstream genes involved in cell expansion, cell division, cold tolerance, and grain yield. Solid and dotted lines ending with a bar indicate direct and indirect repression, respectively. Red crosses indicate the blocked suppressive function of VIG1 and OsbZIP18. Dark green ellipses overlapped indicate the leucine zipper region (ZIP) of VIG1. The VIG1 and OsbZIP18 proteins with normal functions are indicated by the green and yellow circles, respectively. The vig1a and OsbZIP18 proteins with abnormal functions are indicated by the black circles, respectively. The vig1b protein is indicated by the gray circle. Green and gray seedlings represent survival and dead seedlings after chilling stress treatment, respectively. The number of wavy lines indicate the gene expression levels.

To knockout *VIG1*, *OsbZIP18*, or *OsbZIP48*, respectively, a 20-bp carefully designed target was selected from two different parts of the second exon of *VIG1*, the first and third exon of *OsbZIP18*, and the first and second exon of *OsbZIP48* by the CRISPR-GE genome editing tool (http://skl.scau.edu.cn/), and ligated to the CRISPR/Cas9 vector pHUN4C12[31] to obtain the complete CRISPR/Cas9/sgRNA vectors.

To overexpress *VIG1*, the 612 bp full length coding sequence including complete 5′ UTR and 3′UTR of *VIG1* gene was amplified from rice root cDNA using the *VIG1*-OE primers, and ligated to the pZH2Bi vector driven by the ubiquitin promoter.

To overexpress *OsbZIP18*, the 600 bp full length coding sequence of *OsbZIP18* gene was amplified from rice root cDNA using the *OsbZIP18*-OE primers, and ligated to the pZH2Bi vector driven by the ubiquitin promoter.

The resulting vectors were transformed into different materials in the *Agrobacterium tumefaciens*-mediated transformation method. For the knockout assay, the T_1 plants were screened and those lines without exogenous DNA were selected. From these plants, the homozygous mutants were obtained, and the offspring of these mutants were taken for phenotypic investigation. Primers used for vector construction and transformant selection are listed in Supplementary Data 1.

RNA extraction and RT-qPCR analysis

For spatio-temporal expression, samples were taken from shoots and roots of 14-day-old seedlings, and flag leaf blade, flag leaf sheath, internode, and node at the booting stage, as well as young inflorescence and mature floret before anthesis. For transcriptome data verification, samples were taken from shoots of seven-day-old seedlings, and from flag leaf blades, 1-2 mm young panicles before anthesis. Total RNA was extracted using RNAiso PLUS reagent (Takara, No. 9109), and first-strand cDNA was synthesized from 1 μg total RNA using the reverse transcription kit (Promega, No. A3500), according to the manufacturer's instructions after digestion with RNase-free DNase I (Thermo Scientific, No. EN0521). Real-time PCR was performed on the Light Cycler Nano system (Roche) using the SYBR qPCR Mix kit (Roche, No. 04913850001) with three biological replicates for each analysis. *OsActin1* was taken as the internal control for normalization. The relative quantification method ($2^{-\Delta\Delta CT}$) was used to evaluate the quantitative variation of expression[53]. The primers used are listed in Supplementary Data 1.

Yeast two-hybrid assay

The full-length coding sequences of *VIG1*, *vig1a*, *vig1b*, *OsbZIP18*, *OsbZIP48*, and the truncated *VIG1* fragments were amplified from rice root cDNA, respectively, and cloned into the pGADT7 or pGBKT7 vector (Clontech, PT4084-1), all resulting plasmids and the corresponding empty vectors were then co-transformed into the yeast strain Golden Yeast with correct combinations according to the Yeast Two-Hybrid System User Manual (Clontech, PT4084-1). Interactions were detected on SD/-Leu-Trp-His-Ade medium. Primers used in this assay are listed in Supplementary Data 1.

Yeast one-hybrid analysis

Sense and antisense oligonucleotides containing the promoter fragment of *EXPB4*, *EXLA2*, *CYCD1-2*, *OsDREB1A*, *OsDREB1B*, and *OsPID* or a mutated version were designed. Then, sense and antisense nucleotides were annealed and ligated into the pHISi plasmid (Clontech, PT1031-1) to construct the corresponding reporter vector. To generate the reporter, the coding sequence of *VIG1* and *OsbZIP18* were fused with

the GAL4 activation domain of pGAD424 (Clontech, PT1031-1), forming pGAD424-VIG1 or pGAD424-OsbZIP18. The resulting plasmids were co-transformed into the yeast strain YM4271, and DNA-protein interactions were determined according to the growth of transformants on the SD/-His-Leu plates supplied with specific concentration of 3-amino-1,2,4-triazole (3-AT) (Lablead, No. A8056), following the manufacturer's manual (Clontech, PT1031-1). Primers used in this assay are listed in Supplementary Data 1.

GST pull-down assays

The coding sequence of *VIG1*, *vig1a*, and *vig1b* were amplified from rice root cDNA and cloned into the pMAL-c5X to construct MBP-VIG1, MBP-vig1a, and MBP-vig1b vectors, respectively, and the coding sequence of *OsbZIP18* was inserted into the pGEX-4T-1 to form the GST-OsbZIP18 vector. All resulting plasmids were transformed into the *Escherichia coli* strain BL21 and fusion proteins were induced with 0.2 mM IPTG at 28 °C for 12 h. The mouse monoclonal anti-GST (Proteintech, Cat No. 66001-2-Ig, Clone No. 3G12B10) and anti-MBP (Proteintech, Cat No. 66003-1-Ig, Clone No. 4C6H4) antibodies were diluted 1:5000 and 1:2000, respectively, and used in immunoblotting analysis. The HRP-conjugated goat anti-mouse IgG antibody (Proteintech, Cat No. SA00001-1) was diluted 1:10000, and used in immunoblotting analysis. The PageRuler plus prestained protein ladder (Thermo Fisher Scientific, Cat No. 26619) was used as the protein marker. GST pull-down assay was performed following the manufacturer's instructions (Promega, No. V8870). Primers used in this assay are listed in Supplementary Data 1.

Confocal laser scanning microscopy

For subcellular localization, the coding sequence of *VIG1*, *vig1a*, *vig1m1*, *vig1m2*, *vig1m3*, *OsbZIP18*, and *OsbZIP18*-A1 was amplified and inserted into the pSAT6-EYFP-N1 vector (PSAT6) through enzyme digestion and ligation to construct the *VIG1-EYFP* (VIG1-PSAT6), *vig1a-EYFP* (vig1a-PSAT6), *vig1m1-EYFP* (vig1m1-PSAT6), *vig1m2-EYFP* (vig1m2-PSAT6), *vig1m3-EYFP* (vig1m3-PSAT6), *OsbZIP18-EYFP* (OsbZIP18-PSAT6), and *OsbZIP18*-A1-*EYFP* (OsbZIP18-A1-PSAT6) vectors, respectively. The empty vector was used as the negative control. OsbZIP52-mRFP was taken as the nuclear localization marker. The resulting vectors and control constructs were co-transformed into rice protoplasts. For the BiFC assay, the coding sequences of *VIG1*, *vig1a*, *vig1m1*, *vig1m2*, *vig1m3*, *OsbZIP18*, *OsbZIP18*-A1, and *OsbZIP48* were cloned into the pUC19-VYNE (R) and pUC19-VYCE (R) vectors and fused with either N- or C-terminus of the Venus YFP sequence, respectively. The plasmids and corresponding empty vectors were co-transformed in different combinations into rice protoplasts. After 28 °C incubation for 16 h in the dark, the fluorescent signal was detected via a confocal laser scanning microscopy (Leica TCS SP5). All primers used are listed in Supplementary Data 1.

Transient expression assay

For transient expression assay, the above-mentioned VIG1-PSAT6, vig1a-PSAT6, and OsbZIP18-PSAT6 were used as the effector. The 386-bp, 499-bp, 1368-bp, 1053-bp, 1242-bp, 805-bp, and 256-bp promoter region of genes *EXPB4*, *EXLA2*, *CYCD1-2*, *OsDREB1A*, *OsDREB1B*, *Ehd1*, and *OsPID* comprising the putative *cis*-elements were amplified from rice genomic DNA, respectively, and cloned into pGreenII-0800 to construct the reporter vectors. As the internal control, the Renilla LUC vectors were co-transformed with the resulting constructs into rice protoplasts. All transformations were conducted through the PEG-mediated method. After 16 h incubation at 28 °C in the dark, protoplasts were collected as described in the Dual-Luciferase® Reporter Assay System Manual (Promega, No. E1910), and the relative LUC/REN ratio was measured with a luminometer (GLOMAX, Promega). All transient expression assays were performed with three replicates and obtained similar results. Primers used in these assays are listed in Supplementary Data 1.

5′ RACE assay

For examination of the alternative splicing of gene *VIG1* and *OsbZIP18*, 4-day-old shoots of *vig1b*, *VIG1*-NK, and *VIG1*-CK were detached, and total RNA was extracted using RNAiso PLUS reagent (Takara, No. 9109). The resulting total RNA was used in the 5′ RACE conducted according to the manufacturer's instructions (Bingene, No. 220507-10). The KOD plus enzyme with high PCR fidelity (TOYOBO, No. KOD-201) was used for amplification. Primers used in this assay are listed in Supplementary Data 1.

Electrophoretic mobility shift assay (EMSA)

Sense and antisense oligonucleotides containing the G-box (CACGTG) *cis*-element of *EXPB4*, G-box (CACGTG) *cis*-element of *EXLA2*, A-box (TACGTA) *cis*-element of *CYCD1-2*, C-box (GACGTC) *cis*-element of *OsDREB1A*, A-box (TACGTA) *cis*-element of *OsDREB1B*, and G-box (CACGTG) *cis*-element of *OsPID* or a mutated version were synthesized and biotin labeled at the 5′ end to produce the hot probes and mutated probes, respectively. And the same sense and antisense oligonucleotides were synthesized without biotin label to be the competitive probes. The VIG1-MBP and OsbZIP18-GST fusion protein were expressed in the *Escherichia coli* strain BL21 and purified using amylose resin (BioLabs) affinity chromatography. The EMSA was conducted following the manufacturer's instructions by using the LightShift Chemiluminescent EMSA Kit (No. 20148, ThermoFisher SCIENTIFIC). All biotin-labeled primers were synthesized by RuiBiotech (Beijing, China). Photos were taken via Charge-coupled device (CCD) camera. The primers and probe sequences used for EMSA are listed in Supplementary Data 1.

Phylogenetic analysis

The entire amino-acid sequence of VIG1 was used as the query to blast the homologous proteins in the rice genome via the NCBI website (https://blast.ncbi.nlm.nih.gov/Blast.cgi). Phylogenetic trees were constructed with the aligned protein sequences using the MEGA7 software by the neighbor-joining method. Bootstrap values were derived from 1,000 replicates[54]. All the accession numbers for constructing the phylogenetic tree can be found in the Data availability section.

Protein sequence alignment

The protein sequence of VIG1 and their homologous proteins were downloaded from NCBI, and alignments were performed using the ClustalX2.1 software (http://www.clustal.org/download/current/), and combined with Genedoc software (https://www.softpedia.com/get/Science-CAD/GeneDoc.shtml) to generate the results of sequence comparison. The protein sequence alignment among vig1a, VIG1-CK1^{vig1a}, and VIG1-CK2^{vig1a} was conducted via MUltiple Sequence Comparison by Log-Expectation (MUSCLE) database (https://www.ebi.ac.uk/jdispatcher/msa/muscle).

Transcriptome analysis

Seven-day-old shoots of eight seedlings of WT, *vig1a*, and *vig1b* grown in the phytotron (SANYO) with 12 h light (28 °C)/12 h dark (28 °C), 65–70% relative humidity and 150 μM m^{-2} s^{-1} photon flux density were sampled. Total RNA was extracted using the TRIzol reagent according to the manufacturer's protocol (Takara, No. 108-95-2). RNA purity and quantification were evaluated using the NanoDrop 2000 spectrophotometer (Thermo Scientific, USA). RNA integrity was assessed using the Agilent 2100 Bioanalyzer (Agilent Technologies, Santa Clara, CA, USA). Then the libraries were constructed using the TruSeq Stranded mRNA LT Sample Prep Kit (Illumina, San Diego, CA, USA) according to the manufacturer's instructions. The transcriptome sequencing and analysis were conducted by OE Biotech Co., Ltd. (Shanghai, China). The libraries were sequenced on an Illumina HiSeq X Ten platform and 150-bp paired-end reads were generated. Raw data (raw reads) of fastq

format were processed using Trimmomatic[55] (http://www.usadellab.org/cms/index.php?page=trimmomatic), and the clean reads were obtained and mapped to the rice reference genome Os-Nipponbare-Reference-IRGSP-1.0 using HISAT2[56] (http://www.ccb.jhu.edu/software/hisat/). Differential expression analysis was performed using the DESeq (2012) R package[57]. *P*-value < 0.05 and fold change > 2 or fold change <0.5 was set as the threshold for significantly differential expression. The Clustering analysis of the DEGs was performed in the chiplot website (https://www.chiplot.online/heatmap.html). In summary, compared to the WT, a total of 1268 and 595 differentially expressed genes were identified in *vig1a* and *vig1b*, respectively.

Reporting summary

Further information on research design is available in the Nature Portfolio Reporting Summary linked to this article.

Data availability

Data supporting the findings are available within this paper and its Supplementary Information files. The transcriptome data generated in this study have been deposited in the NCBI/Sequence Read Archive (SRA) database under accession PRJNA1098560. Gene sequences from this article can be found in the Rice Annotation Project (RAP) database (http://rice.uga.edu/index.shtml). Source data are provided with this paper.

References

1. Sasaki, T. & Burr, B. International Rice Genome Sequencing Project: the effort to completely sequence the rice genome. *Curr. Opin. Plant Biol.* **3**, 138–141 (2000).
2. Wei, S. et al. A transcriptional regulator that boosts grain yields and shortens the growth duration of rice. *Science* **377**, eabi8455 (2022).
3. Smith, K. et al. Meeting the global protein supply requirements of a growing and ageing population. *Eur. J. Nutr.* **63**, 1425–1433 (2024).
4. Li, X., Dong, J., Zhu, W., Zhao, J. & Zhou, L. Progress in the study of functional genes related to direct seeding of rice. *Mol. Breeding* **43**, 46 (2023).
5. Mahender, A., Anandan, A. & Pradhan, S. K. Early seedling vigour, an imperative trait for direct-seeded rice: an overview on physio-morphological parameters and molecular markers. *Planta* **241**, 1027–1050 (2015).
6. Huang, X. et al. A map of rice genome variation reveals the origin of cultivated rice. *Nature* **490**, 497–501 (2012).
7. Zhang, J., Li, X. M., Lin, H. X. & Chong, K. Crop improvement through temperature resilience. *Annu. Rev. Plant. Bio.* **70**, 753–780 (2019).
8. Dimaano, N. G. B. et al. Identification of quantitative trait loci governing early germination and seedling vigor traits related to weed competitive ability in rice. *Euphytica* **216**, 159 (2020).
9. Ma, Y. et al. Genome-wide association mapping and gene expression analysis identify *OsCPS1* as a new candidate gene controlling early seedling length in rice. *Front. Plant Sci.* **13**, 976669 (2022).
10. Wang, F. et al. Genome-wide association and gene validation studies for early root vigour to improve direct seeding of rice. *Plant Cell Environ.* **41**, 2731–2743 (2018).
11. Chen, K. et al. Genetic dissection of seedling vigour in a diverse panel from the 3000 Rice (*Oryza sativa* L.) Genome Project. *Sci. Rep.* **9**, 4804 (2019).
12. Yang, J. et al. Quantitative trait locus analysis of seed germination and early seedling growth in rice. *Front. Plant Sci.* **10**, 1582 (2019).
13. Zhang, H. et al. Genome-wide association study of root system development at seedling stage in rice. *Genes* **11**, 1395 (2020).
14. Chen, H. et al. E3 ubiquitin ligase SOR1 regulates ethylene response in rice root by modulating stability of Aux/IAA protein. *Proc. Natl Acad. Sci. USA* **115**, 4513–4518 (2018).
15. Morii, M. et al. The dual function of OsSWEET3a as a gibberellin and glucose transporter is important for young shoot development in rice. *Plant and Cell Physiol.* **61**, 1935–1945 (2020).
16. Fujino, K. et al. Molecular identification of a major quantitative trait locus, *qLTG3-1*, controlling low-temperature germinability in rice. *Proc. Natl Acad. Sci. USA* **105**, 12623–12628 (2008).
17. Ma, Y. et al. *COLD1* confers chilling tolerance in rice. *Cell* **160**, 1209–1221 (2015).
18. Liu, C. et al. Early selection of *bZIP73* facilitated adaptation of *japonica* rice to cold climates. *Nat. Commun.* **9**, 3302 (2018).
19. Zhang, Z. et al. Natural variation in *CTB4a* enhances rice adaptation to cold habitats. *Nat. Commun.* **8**, 14788 (2017).
20. Zhang, Z. et al. OsMAPK3 phosphorylates OsbHLH002/OsICE1 and inhibits its ubiquitination to activate *OsTPP1* and enhances rice chilling tolerance. *Dev. Cell* **43**, 731–743.e735 (2017).
21. Chen, L. et al. OsMADS57 together with OsTB1 coordinates transcription of its target *OsWRKY94* and *D14* to switch its organogenesis to defense for cold adaptation in rice. *N. Phytol.* **218**, 219–231 (2018).
22. Ge, Q. et al. Cyclophilin OsCYP20-2 with a novel variant integrates defense and cell elongation for chilling response in rice. *N. Phytol.* **225**, 2453–2467 (2020).
23. Li, Z. et al. OsGRF6 interacts with SLR1 to regulate *OsGA2ox1* expression for coordinating chilling tolerance and growth in rice. *J. Plant Physiol.* **260**, 153406 (2021).
24. Xing, Y. & Zhang, Q. Genetic and molecular bases of rice yield. *Annu. Rev. Plant Biol.* **61**, 421–442 (2010).
25. Zhang, D. & Yuan, Z. Molecular control of grass inflorescence development. *Annu. Rev. Plant Biol.* **65**, 553–578 (2014).
26. Ashikari, M. et al. Cytokinin oxidase regulates rice grain production. *Science* **309**, 741–745 (2005).
27. Huang, X. et al. Natural variation at the *DEP1* locus enhances grain yield in rice. *Nat. Genet.* **41**, 494–497 (2009).
28. Jiao, Y. et al. Regulation of *OsSPL14* by OsmiR156 defines ideal plant architecture in rice. *Nat. Genet.* **42**, 541–544 (2010).
29. He, Y. et al. *IPA1* negatively regulates early rice seedling development by interfering with starch metabolism via the GA and *WRKY* pathways. *Int. J. Mol. Sci.* **22**, 6605 (2021).
30. Jia, M. et al. Chilling-induced phosphorylation of IPA1 by OsSAPK6 activates chilling tolerance responses in rice. *Cell Discov.* **8**, 71 (2022).
31. Xie, X. et al. CRISPR-GE: a convenient software toolkit for CRISPR-based genome editing. *Mol. Plant* **10**, 1246–1249 (2017).
32. Osterlund, M. T., Hardtke, C. S., Wei, N. & Deng, X. W. Targeted destabilization of HY5 during light-regulated development of *Arabidopsis*. *Nature* **405**, 462–466 (2000).
33. Holm, M., Ma, L. G., Qu, L. J. & Deng, X. W. Two interacting bZIP proteins are direct targets of COP1-mediated control of light-dependent gene expression in *Arabidopsis*. *Genes Dev.* **16**, 1247–1259 (2002).
34. Bhatnagar, A. et al. Two splice forms of *OsbZIP1*, a homolog of *AtHY5*, function to regulate skotomorphogenesis and photomorphogenesis in rice. *Plant Physiol.* **193**, 426–447 (2023).
35. Chai, J. et al. OsRE1 interacts with OsRIP1 to regulate rice heading date by finely modulating *Ehd1* expression. *Plant Biotechnol. J.* **19**, 300–310 (2021).
36. Li, S. et al. Improving yield-related traits by editing the promoter of the heading date gene *Ehd1* in rice. *Theor. Appl. Genet.* **136**, 239 (2023).
37. Wu, H. M., Xie, D. J., Tang, Z. S., Shi, D. Q. & Yang, W. C. PINOID regulates floral organ development by modulating auxin transport and interacts with MADS16 in rice. *Plant Biotechnol. J.* **18**, 1778–1795 (2020).
38. Foster, R., Izawa, T. & Chua, N. H. Plant bZIP proteins gather at ACGT elements. *The FASEB J.* **8**, 192–200 (1994).
39. Hasegawa, T. et al. Mutation of *OUR1*/*OsbZIP1*, which encodes a member of the basic leucine zipper transcription factor family,

promotes root development in rice through repressing auxin signaling. *Plant Sci.* **306**, 110861 (2021).
40. Tanaka, N. et al. OsbZIP1 regulates phosphorus uptake and nitrogen utilization, contributing to improved yield. *Plant J.* **118**, 159–170 (2024).
41. Doi, K. et al. *Ehd1*, a B-type response regulator in rice, confers short-day promotion of flowering and controls *FT*-like gene expression independently of *Hd1*. *Genes Dev.* **18**, 926–936 (2004).
42. Wu, Y. et al. The QTL *GNP1* encodes GA20ox1, which increases grain number and yield by increasing cytokinin activity in rice panicle meristems. *PLoS Genet.* **12**, e1006386 (2016).
43. Zhang, G., Xu, N., Chen, H., Wang, G. & Huang, J. *OsMADS25* regulates root system development via auxin signalling in rice. *Plant J.* **95**, 1004–1022 (2018).
44. Lv, Y. et al. Targeted mutagenesis of *POLYAMINE OXIDASE 5* that negatively regulates mesocotyl elongation enables the generation of direct-seeding rice with improved grain yield. *Mol. Plant* **14**, 344–351 (2021).
45. Dubouzet, J. G. et al. *OsDREB* genes in rice, *Oryza sativa* L., encode transcription activators that function in drought-, high-salt- and cold-responsive gene expression. *Plant J.* **33**, 751–763 (2003).
46. Bai, X. et al. Duplication of an upstream silencer of *FZP* increases grain yield in rice. *Nat. Plants* **3**, 885–893 (2017).
47. Wang, J. et al. A single transcription factor promotes both yield and immunity in rice. *Science* **361**, 1026–1028 (2018).
48. Catalá, R., Medina, J. & Salinas, J. Integration of low temperature and light signaling during cold acclimation response in *Arabidopsis*. *Proc. Natl Acad. Sci. USA* **108**, 16475–16480 (2011).
49. Sun, Y. et al. Natural variation in the *OsbZIP18* promoter contributes to branched-chain amino acid levels in rice. *N. Phytol.* **228**, 1548–1558 (2020).
50. Burman, N., Bhatnagar, A. & Khurana, J. P. OsbZIP48, a HY5 transcription factor ortholog, exerts pleiotropic effects in light-regulated development. *Plant Physiol.* **176**, 1262–1285 (2017).
51. Li, Y., Zheng, L., Corke, F., Smith, C. & Bevan, M. W. Control of final seed and organ size by the *DA1* gene family in *Arabidopsis thaliana*. *Genes Dev.* **22**, 1331–1336 (2008).
52. Xu, Y. et al. Natural variations of *SLG1* confer high-temperature tolerance in *indica* rice. *Nat. Commun.* **11**, 5441 (2020).
53. Livak, K. J. & Schmittgen, T. D. Analysis of relative gene expression data using real-time quantitative PCR and the $2^{-\Delta\Delta C}_{T}$ method. *Methods* **25**, 402–408 (2001).
54. Kumar, S., Stecher, G. & Tamura, K. MEGA7: molecular evolutionary genetics analysis version 7.0 for bigger datasets. *Mol. Biol. Evol.* **33**, 1870–1874 (2016).
55. Bolger, A. M., Lohse, M. & Usadel, B. Trimmomatic: a flexible trimmer for Illumina sequence data. *Bioinformatics* **30**, 2114–2120 (2014).
56. Kim, D., Langmead, B. & Salzberg, S. L. HISAT: a fast spliced aligner with low memory requirements. *Nat. Methods* **12**, 357–360 (2015).
57. Anders, S. & Huber, W. European. Differential expression of RNA-Seq data at the gene level-the DESeq package. *EMBL* (2012). [http://www.bioconductor.org/packages/devel/bioc/vignettes/DESeq/inst/doc/DESeq.pdf].

Acknowledgements

We greatly thank Professor Yaoguang Liu (SCAU) for generously providing the CRISPR/Cas9 genome editing vector pHUN4C12. We greatly thank Professor Chengcai Chu (SCAU) for generously offering the vector of nuclear localization marker OsbZIP52-mRFP and the luciferase reporter vector pGreenII-0800. This work was supported by grants from the Strategic Priority Research Program of the Chinese Academy of Sciences (XDA24030201), and the State Key Laboratory of Plant Genomics (SKLPG2011B0403).

Author contributions

S.Y. supervised the project. S.Y. and D.X. designed the research. J.W. conducted the map-based cloning of *VIG1*. R.W. screened the *vig1a* and *vig1b* mutants, and performed field management. Y.W. contributed to the reagents and equipment support. Y.L. and G.S. assisted in the data collection. D.X. performed the experiments, analyzed the data and prepared the original draft. S.Y. revised the manuscript.

Competing interests

The authors declare no competing interests.

Additional information

Supplementary information The online version contains supplementary material available at https://doi.org/10.1038/s41467-024-52510-3.

Correspondence and requests for materials should be addressed to Shanguo Yao.

Peer review information *Nature Communications* thanks the anonymous reviewers for their contribution to the peer review of this work. A peer review file is available.

Reprints and permissions information is available at http://www.nature.com/reprints

Publisher's note Springer Nature remains neutral with regard to jurisdictional claims in published maps and institutional affiliations.

Open Access This article is licensed under a Creative Commons Attribution-NonCommercial-NoDerivatives 4.0 International License, which permits any non-commercial use, sharing, distribution and reproduction in any medium or format, as long as you give appropriate credit to the original author(s) and the source, provide a link to the Creative Commons licence, and indicate if you modified the licensed material. You do not have permission under this licence to share adapted material derived from this article or parts of it. The images or other third party material in this article are included in the article's Creative Commons licence, unless indicated otherwise in a credit line to the material. If material is not included in the article's Creative Commons licence and your intended use is not permitted by statutory regulation or exceeds the permitted use, you will need to obtain permission directly from the copyright holder. To view a copy of this licence, visit http://creativecommons.org/licenses/by-nc-nd/4.0/.

© The Author(s) 2024